Modeling heme proteins using atomistic simulations†

Damián E. Bikiel,[a] Leonardo Boechi,[a] Luciana Capece,[a] Alejandro Crespo,[a] Pablo M. De Biase,[a] Santiago Di Lella,[ab] Mariano C. González Lebrero,[a] Marcelo A. Martí,[a] Alejandro D. Nadra,[a] Laura L. Perissinotti,[a] Damián A. Scherlis[a] and Darío A. Estrin*[a]

Received 14th August 2006, Accepted 28th September 2006
First published as an Advance Article on the web 11th October 2006
DOI: 10.1039/b611741b

Heme proteins are found in all living organisms, and perform a wide variety of tasks ranging from electron transport, to the oxidation of organic compounds, to the sensing and transport of small molecules. In this work we review the application of classical and quantum-mechanical atomistic simulation tools to the investigation of several relevant issues in heme proteins chemistry: (i) conformational analysis, ligand migration, and solvation effects studied using classical molecular dynamics simulations; (ii) electronic structure and spin state energetics of the active sites explored using quantum-mechanics (QM) methods; (iii) the interaction of heme proteins with small ligands studied through hybrid quantum mechanics–molecular mechanics (QM-MM) techniques; (iv) and finally chemical reactivity and catalysis tackled by a combination of quantum and classical tools.

1. Introduction

Heme proteins, the family of proteins containing an iron–porphyrin complex as a prosthetic group, are found in all living organisms.[1] They perform a wide variety of tasks ranging from electron transport,[2] to the oxidation of organic compounds,[3] to the sensing and transport of small molecules, namely O_2, CO and NO.[4] The heme group consists of a porphyrin macrocycle containing a central iron atom coordinated to four in-plane nitrogen atoms (Scheme 1).

Typically, the metal forms one or two additional axial bonds, below and above the molecular plane, which may connect the prosthetic group to the rest of the protein. These axial sites available for coordination are known as proximal and distal sites (shown above and below the heme, respectively, in Scheme 2). When only one of these sites is occupied the heme is said to be pentacoordinated (5c), with the distal site free. In some heme proteins, commonly in those involved in electron transport, there is another residue occupying the distal site and the heme is hexacoordinated (6c). Residues acting as heme ligands are mostly His, Cys, Met, Lys or Tyr. The investigation of heme proteins is of interest due to their widespread occurrence among diverse species as well as to their multiple functions, which in many cases remain unexplained.

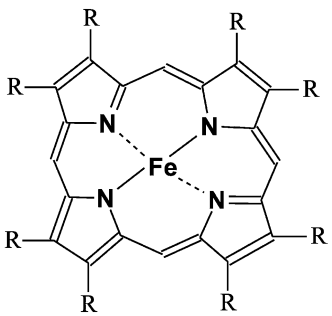

Scheme 1 Iron porphyrin.

Computational techniques for modeling large biological molecules have emerged during the last decades as an important tool to complement experimental information. The *in silico* generated models and the information which can be obtained throughout their study are essential for analyzing the structural and kinetic data provided by the experimental methods. In particular, computer simulations allow a systematic and economical tool to analyze the dependence of a property of interest on static (*e.g.* aminoacid sequence) and

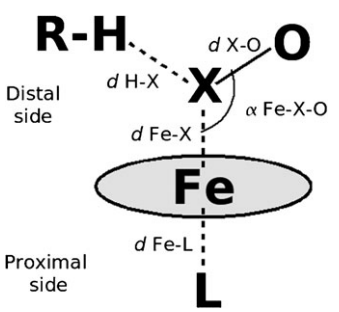

Scheme 2 Representation of heme active sites.

[a] *Departamento de Química Inorgánica, Analítica y Química Física/ INQUIMAE-CONICET, Facultad de Ciencias Exactas y Naturales, Universidad de Buenos Aires, Ciudad Universitaria, Pabellón II, Buenos Aires, (C1428EHA), Argentina. E-mail: dario@qi.fcen.uba.ar; Fax: (5411)4576-3341; Tel: (5411)4576-3378*
[b] *Instituto Superior de Investigaciones Biológicas (INSIBIO), CONICET- Facultad de Bioquímica, Química y Farmacia, Universidad Nacional de Tucumán, Chacabuco 461, San Miguel de Tucumán, (T4000ILI), Argentina*

† The HTML version of this article has been enhanced with colour images.

dynamical factors. In the recent years, the increase in the computing power and in the accuracy of the models, made possible in many cases to draw biologically relevant conclusions and propose new hypothesis based mainly on computer generated data. Due to the fact that all heme proteins share the same active site, and that their chemical reactivity and function are subtly modulated by the protein environment, heme proteins constitute also ideal benchmarks for many computational techniques.

The modeling of phenomena which do not involve formation or breaking of chemical bonds may be achieved, in principle, without resorting to quantum mechanics, by employing classical force fields (even though such force fields often contain parameters based on quantum-mechanical calculations). Among the most widely used force fields for biomolecules we can mention Amber,[5] Charmm,[6] and Gromos.[7] The time scale accessible in atomistic simulations with modern hardware technology is limited to the nanoseconds/microseconds range, yet the predictive power of simulation schemes has increased enormously in the last years by the development of advanced sampling techniques.[8–10] Classical simulation techniques are not able to deal with reactive processes where covalent chemical bonds are being formed or broken, in which cases it is necessary to employ quantum-mechanics (QM) schemes. There are two main strategies to tackle chemical processes in biomolecules. One is based on electronic structure calculations using appropriate model systems of moderate size, typically including the active site plus eventually the most relevant region of the environment. The second strategy is to employ hybrid quantum mechanical–molecular mechanical (QM-MM) methods. These are adequate for the investigation of chemical events that take place in a limited region of a large system (the QM region), to be modelled using QM at a certain level of theory, which may range from simplified valence bond schemes, to semiempirical methods, to Hartree–Fock and density functional theory (DFT).[11–13] The remainder of the system (MM region) is treated at the less expensive molecular mechanics, or classical, level. The use of this kind of techniques for the investigation of chemical reactivity in solution and in enzymes has become very popular in the last years.

In this work we discuss selected results on classical and quantum-mechanical computer simulations of heme proteins. In section 2, results obtained using classical molecular dynamics simulations are presented. Section 3 refers to the electronic structure and the spin states of heme active sites, with an emphasis on the suitability of the QM techniques to treat this problem. Section 4 is devoted to the interaction of heme proteins with small ligands, namely O_2, CO, NO, and HNO. Finally, in section 5 we focus on the discussion concerning the catalytic function performed by several heme proteins.

2. Classical molecular dynamics simulations of heme proteins

In this section selected examples are presented that illustrate the possible applications of molecular dynamics (MD) simulations to get insight on structural and dynamical aspects of heme proteins.

2.1 Conformational analysis

Myoglobin (Mb), a monomeric heme protein that gives muscle its red color and stores oxygen at the heme group, has been the subject of numerous theoretical and experimental studies in the last decades. In spite of this plethora of research, Mb is still not fully understood, and other roles than oxygen storage have been proposed recently.

Myoglobin is one of the most studied proteins employing computer simulation. A pioneering MD work developed on myoglobin provided the first direct demonstration that there is a large number of thermally accessible minima in the vicinity of the native structure obtained by means of crystallography.[14] Conformational changes have been thereafter thoroughly investigated in myoglobin, and also in other globins and in several cytochromes. Classical molecular dynamics simulations have been employed to describe the processes involved in the folding and unfolding of apomyoglobin (the protein without the heme group), allowing to analyze fluctuations and identify labile and non labile regions.[15,16] Other groups have focused on the identification of the changes produced in the native myoglobin, monitoring motions in the active site in order to understand the experimentally observed nonexponential relaxation after ligand photodissociation,[17,18] and the conformational changes experimented by the photodissociated carbonmonoxymyoglobin.[19] Temperature effects on myoglobin dynamics and structure were the subject of several studies as well. In particular, it was shown that under the glass-like transition temperature (around 210 K) the protein is trapped in restricted regions of the conformational space, while above this temperature a much larger region is accessible, including backbone dihedral angles that were restricted at lower temperatures.[20,21] The effects of heme rotational isomerism in sperm-whale carbonmonoxy myoglobin have been assessed by means of MD simulations. The results showed that the protein matrix induced similar heme distortions in the two possible heme conformations.[22] In the same context, the heme conformation has been found to correlate with the conformational dynamics of the protein on a time scale of hundreds of picoseconds, suggesting that the heme conformation may provide a useful probe of dynamical processes in the protein.[23]

Electron transfer processes are some of the more important tasks performed by heme proteins, and were the subject of many experimental and theoretical papers in the last years. We mention here the recent MD simulations by Oliveira *et al.*[24] focused on the redox processes in tetraheme cytochrome c3. In their work, multiple simulations of two different lengths (4 ns and 50 ps) were run for both the oxidized and the reduced states of the cytochrome. The perturbation of the system to go from the oxidized to the reduced forms by means of the subtraction technique (a nonequilibrium approach), made possible the characterization of the conformational changes at different timescales and the computation of the free energy of reduction of each individual heme,[25] as well as the interaction energy terms between the different heme units.[26]

As a whole, these experiments greatly contributed to the understanding of protein dynamics beyond its structure, and provided clues about the role and the relevance of particular regions with respect to protein function.

2.2 Cavities and ligand migration

The function of many heme proteins is intimately related to the interaction of the heme active site with small diatomic ligands such as O_2, CO and NO, and may also require the presence of more complex substrates. This makes the investigation of ligand migration across the protein matrix a key issue for understanding the molecular basis of protein function. Although the term "ligand diffusion" is usually found in the literature to describe the motion of ligands within the protein, it is probably more accurate to use the term ligand migration to refer to these non-stochastic phenomena.

Molecular dynamics offers an ideal tool for the investigation of cavities and migration within them: it was applied in several cases to follow the evolution of the ligand in the distal cavity of the heme[18,27,28] and in the protein matrix[17,29,30] of myoglobin, and to characterize the pattern of structural fluctuations associated with protein motion that interconnect and isolate the different cavities, thus controlling ligand migration.[31] MD simulations made possible the identification of channels in P450cam,[32] that were not evident from the experimental crystal structures. Bossa *et al.*[33,34] reported an extended simulation (>80 ns) on CO migration in wild type Mb and mutants, in a time scale comparable with experimental (time resolved X-ray) data, unveiling migration pathways and showing how the presence of a diatomic ligand may affect structural fluctuations enhancing the probability of opening cavity-connecting channels. Protein fluctuations are influenced by the ligand in such a way that the opening and closure of a passage between adjacent cavities is strictly correlated to its presence. Since ligand migration times can be much longer than the cavity's lifetime, ligand passages remain closed most of the time, and open progressively as the ligand goes along. In thermodynamical terms, Sheu[35] has shown that the process of ligand escape is basically entropy driven. The role of side chain motions[36] in the active site of myoglobin on the overall rate of O_2 dissociation has been established by MD simulations, and has been found to be controlled by the hydrogen bond between the bound ligand an the distal histidine residue, but also by fast fluctuations of internal sidechains, which can either permit or obstruct access of the ligand to cavities within the protein.[36,37]

Standard molecular dynamics at the nanosecond time scale does not always provide a complete representation of the migration of single ligand molecules through non obvious migration pathways. This difficulty can be overcome by the use of different sampling methods to enhance sampling at an affordable computational cost. One of these techniques, activated molecular dynamics (aMD), consists in assigning to the ligand a temperature much higher than that of the rest of the system. Activated molecular dynamics simulations have been employed to investigate water and hydrogen peroxide migration in catalase.[38] An alternative method to enhance sampling is based on the application of an artificial randomly oriented force on the substrate. This methodology was used to deal with relatively large ligands, such as camphor.[39] Other studies have been carried out implementing a technique inspired on the time dependent Hartree approximation, which enhances sampling efficiency combining multiple ligand trajectories with a single protein trajectory.[17] In this approach, several ligands are allowed to evolve inside the protein matrix within the same run. A drawback of this treatment is that specific information about protein-ligand interaction is lost in the average behavior, and that the volume of the cavities is overestimated due to the presence of multiple ligands. As a last example, it is also possible to estimate free-energy profiles and free energy barriers associated with ligand migration by means of umbrella sampling techniques. Using these kinds of schemes, free energy profiles for CO escape were obtained for wild type MbCO and the L29F mutant.[40] Overall, these computational schemes have provided information on the mechanisms of ligand migration that are difficult to obtain using experimental techniques.

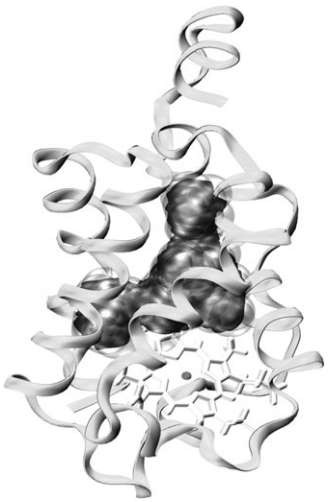

Fig. 1 Schematic representation of truncated hemoglobin N of *Mycobacterium tuberculosis*, which shows the two channels for ligand migration.

Multiple steering molecular dynamics schemes[41] have also been employed to model activated processes such as ligand passage between cavities through a narrow channel. These methods force the ligand to explore energetically unfavorable regions,[42] and are especially suited to calculate free energies associated with the channels and barriers that a ligand must surpass to reach the active site. This strategy was used by Bidon-Chanal *et al.*[43] to investigate the NO-dioxygenase mechanism of truncated hemoglobin N (trHbN) of *Mycobacterium tuberculosis*. X-Ray trHbs structures revealed that trHbN host a tunnel/cavity system, composed of two branches (Fig. 1), connecting the heme moiety with the exterior of the protein, a function probably being associated to controlling ligand diffusion and storage. Extended molecular dynamics simulations were employed to characterize the factors controlling diatomic ligand migration through the apolar tunnel system, suggesting that O_2 migration in deoxy-trHbN is

restricted to the short branch of the tunnel, and that O_2 binding to the heme drives conformational and dynamical fluctuations promoting NO migration through the long tunnel branch. Thus, the computational results obtained by our group suggest that trHbN has evolved a dual-path mechanism for distinctive migration of O_2 and NO to the heme to achieve the most efficient NO detoxification. The energetic barriers associated to ligand migration from bulk solvent to the active site, where the reaction is held, have been computed and are consistent with the available kinetic information.[43] Two different truncated hemoglobins, known as trHbO and trHBN, are produced by *M. tuberculosis*. Recent results from the Bolognesi and Guertin's groups show that trHbN appears to be better suited for performing NO/O_2 chemistry, actively detoxifying NO and yielding the innocuous nitrate as product.[44,45]

The current picture of internal cavities and ligand passageways is that cavities appear and disappear dynamically. The more persistent cavities usually correspond to the so called "xenon docking sites", observed in X-ray experiments of proteins crystallized in the presence of this gas. The existence of cavities and docking sites often depends on fine details of the structure, to the extent that proteins having similar folds do not necessarily share the same features concerning ligand migration.[46]

2.3 Quaternary structure and protein–protein interactions

One interesting problem in which classical molecular dynamics simulations appear particularly useful is the communication between subunits in multi domain heme proteins. The paradigmatic example of an allosteric multi subunit heme protein is the mammalian oxygen transport protein, hemoglobin. The hemoglobin molecule is an assembly of four subunits, consisting of two α and two β subunits not covalently bound, denoted as $\alpha_2\beta_2$. Hemoglobin may be found in two major conformations: the R and T states. In the absence of oxygen, the T state is the most stable, and the predominant conformation of Hb. The binding of O_2 induces conformational changes that make the R conformation (which exhibits a much higher affinity for O_2) more stable. Much effort was made in the last decades to gain knowledge of the allosteric effect of this protein. Early simulations of dimers were useful to explain the molecular basis for the transmission of distal heme perturbations across the α1-β1 interface.[47] More recent studies performed using the entire protein,[48] allowed to characterize in detail the structural modifications of Hb during the transition between the T and R states. The computational results showed that the heme does not exhibit any significant movement with respect to the polypetide chain during T-to-R transition. It has been postulated that dimer rotation (a key movement in the T-to-R transition) is not induced directly by ligand binding. According to this hypothesis, the protein has a natural propensity for this movement, probably corresponding to a low frequency mode, but it appears to be limited by the aminoacid backbone in the joint region in the T state. O_2 binding unlocks this clamp, the mode is released and allows the transition to occur. This study confirmed the results obtained previously by the same authors by employing a novel methodology to compute low frequency normal modes. More specifically, the projection of the calculated modes of the T state showed that there is one mode at 2.0 cm^{-1} that has a predominant contribution to the T-to-R transition. The authors also suggested that the opening of the β distal side may be crucial for increasing oxygen affinity.[48]

Another interesting example of cooperative effects modulating oxygen affinity can be found in the *Scapharca inaequivalvis* homodimeric hemoglobin, which is composed of subunits resembling the fold found in Hb. This protein is also highly cooperative, but the effect of structural changes on ligand binding is small. Molecular dynamics simulations (together with spectroscopic data) indicated that the higher oxygen affinity displayed by the Thr-72→Ile mutant is mainly due to a local perturbation in the dimer interface that propagates to the heme region, affecting the polarity of the heme environment and the interactions of the heme propionate groups with the surrounding residues. The number of water molecules entering the dimer interface is lower in the mutant than in the wild-type protein, the two subunits make closer contacts, and distances between specific residues, which have been shown to play a determinant role in the CO or O_2 binding, fluctuate around values similar to those observed in the ligand-bound structure of the wild-type protein. These changes are consistent with a destabilization of the T state and a stabilization of the R state in the mutant relative to the native protein.[49]

More recently, Zhou *et al.*[50] investigated the mechanism of cooperativity in the same protein. Since, unlike human hemoglobin, no structures for intermediates are available, they were constructed by combining subunits from the unligated and ligated dimers. Two structurally distinct intermediates were examined, and it was shown that the transition between the two is directly related to the number of interfacial water molecules. These authors showed that reduction of water (to a dry, oxy-like interface) promotes the conformational change of Phe97 from its deoxy to oxy position. Furthermore, it was found that there is a well-defined water channel connecting the interface between the subunits with bulk water. The bottleneck or gate of the channel, which can be open or closed, has been found to be made of hydrophilic residues.

The structural and dynamical features of more complex heme proteins such as the mitochondrial type I nitric oxide (mtNOS-I) synthase, have also been investigated by means of MD simulations.[51] In that work, the molecular details of the physical interaction between this protein and the C-terminal peptide of the subunit one of Cytochrome c oxidase (CcOX) are analyzed, showing a consensus sequence for binding to the PDZ domain of mtNOS-I previously unreported for CcOX. For the first time a protein–protein interaction mediated by PDZ domains involving CcOX was proposed on the grounds of molecular dynamics simulations.

2.4 Solvation water effects and related studies

Molecular dynamics simulation of heme proteins has been widely used in the study of solvation processes and hydration energetics.[52–54] MD studies allow to obtain parameters such as the average occupancy and the residence time of water

molecules and to shed light on the hydration shell structure and dynamics. Pioneering studies in this area revealed information of hydration sites and helped to assess the importance of hydration in protein stability. Stewart *et al.*[55] analyzed the role of hydration by performing simulations including explicit solvent molecules, and then replacing them by a distance-dependent dielectric constant which approximates the screening effects of bulk water. The tests, done on the complex formed between the tetraheme cytochrome c3 and the iron protein rubredoxin from the sulfate-reducing bacterium *Desulfovibrio vulgaris*, showed that the presence of explicit water molecules provided a significant stabilization effect. Steinbach *et al.*[56] performed MD simulations of myoglobin and found that the protein is fully hydrated by 350 water molecules, in agreement with experiments. The authors also found the formation of water clusters around charged groups during the simulation. The glass transition observed experimentally in hydrated myoglobin near 220 K was also investigated by correlating the transition with an increase in the number of dihedral angles undergoing a qualitative change, from a harmonic to an anharmonic torsional mode. They concluded that the anharmonic protein motions above 220 K are enhanced by protein hydration. Smith *et al.*[57] also explained this phenomenon in terms of water dynamics.

Myoglobin has also been subject of studies as a model to understand the thermodynamics and structural dynamics of water around proteins. Gu *et al.*[58] confirmed that only a few water molecules are tightly bound to protein atoms, while most solvent molecules are labile, continuously experiencing breaking and forming of hydrogen bonds. Makarov *et al.*[59,60] confirmed that there is no direct correlation between the spatial and the temporal (residence time) order of the solvent in the myoglobin hydration shell.

Interesting experiments have been made in coated proteins: Cottone *et al.*[61] worked with carboxy-myoglobin embedded in a water–trehalose system with the goal of studying the importance of the solvent. Several differences with respect to water were noticed: the configuration of the heme is perturbed, and the motional freedom of the loop and helix structures, needed for the protein function and in particular for ligand migration, is largely reduced. More recently,[62] the same research team performed simulations in sucrose- and trehalose-coated carboxy-myoglobin that indicated a different efficiency in bioprotection. Different heme pocket structures are observed in the two systems, and significant differences in the number of water molecules shared between the protein and the sugar were observed along the simulations. The same authors[63] studied the internal dynamics and protein-matrix coupling in a trehalose-coated carboxy derivative of horse heart myoglobin, explaining how water containing matrices control the internal dynamics of the embedded proteins *via* the formation of hydrogen bond networks that anchor the protein surface to the surrounding matrix, whose stiffness increases by lowering the sample water content.

As shown by these experiments, MD appears to be a promising approach to get insight in the poorly understood microscopic behavior of solvent surroundings and its participation in protein stability and function.

2.5 Studying reactive processes with classical dynamics

In principle, the modeling of chemical reactivity requires the use of QM based techniques. However, due to the large computational expense associated with QM methods, in certain cases, some insight about chemical processes may be obtained by using purely classical simulations. Schaad *et al.*[64] considered NO rebinding to Mb using a potential that switched smoothly between a nonbinding and a binding situation. More recently, Meuwly *et al.*[65] treated chemical reactions as surface crossing between two MM surfaces corresponding to the two reactions states (*i.e.* the reactants and the products), establishing the rebinding events according to an energy criterion. This approach was further improved by Nutt *et al.*,[66] who introduced an explicit algorithm to go back and forth between the bound and unbound states.

Classical MD has been used to study a wide range of physicochemical, biophysical and biological problems, ranging from conformational changes to ligand migration. It has shown to be a unique technique to gain details on the microscopic changes and interactions within a macromolecule, complementing and enhancing the profit of experimental approaches.

3. Spin state energetics of the heme active site

The spin state of iron porphyrins, as much as the spin state of any transition metal complex, is determined by the coordination symmetry and the nature of the ligands. In heme proteins, as already mentioned, the iron atom may be found in different environments, typically four-, five-, or six-coordinated, and most frequently exhibiting a formal oxidation state of $+2$ or $+3$, though high-valent species as Fe(IV) have been identified in certain intermediates.[67] Unligated Fe(II) porphyrins have an even number of electrons, therefore the three lowest accessible spin states are a singlet, a triplet and a quintuplet ($S = 0$, 1, and 2, respectively), which become a doublet, a quartet and a sextuplet in Fe(III) porphyrins. These three low-lying states are conventionally referred to as low-, intermediate-, and high-spin. In the unligated heme, the metal is bonded to the four equatorial nitrogen atoms in D_{4h} symmetry. Experimental studies on model systems of the four-coordinated heme,[68–72] namely on Fe(II) tetraphenylporphine (FeTPP), indicated a triplet ground state corresponding to a ^3A_g configuration. Axial ligands perturb the relative energy of the d orbitals, leading to alternative multiplicities, as illustrated in Scheme 3 for a d^6 complex.[73]

Thus, five coordinated iron porphyrins can be encountered in different spin states: imidazole gives rise to high spin hemes, while strong ligand-fields as those of diatomic molecules like CO, NO or O_2, favor low spin configurations.[73] Six-coordinated hemes, with two axial ligands, usually exhibit a low spin state unless the ligand-field is extremely weak. In the oxy hemoglobin, calculations suggest the occurrence of an open shell singlet, arising from the antiferromagnetic coupling of the unpaired electron densities of the O_2 molecule ($S = 1$) and the histidine-coordinated porphyrin ($S = 2$).[74,75] The geometrical features of the metal center are intimately related to the spin state, in particular in high spin, five coordinated hemes,

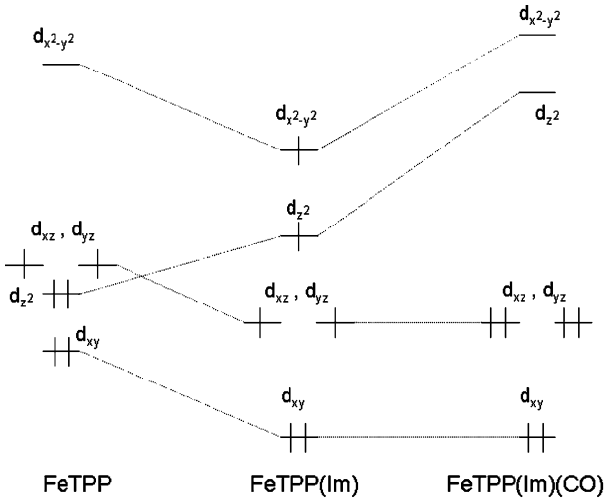

Scheme 3 Qualitative representation of the d-orbitals energy levels for FeTPP: (a) free (four-coordinated); (b) ligated to imidazole (five-coordinated); (c) ligated to imidazole plus CO (six-coordinated).

where the metal atom is significantly displaced from the D_{4h} plane defined by the nitrogens, in some cases, as much as 0.5 Å. This delicate interplay between structure and multiplicity will have important implications in the affinity and the activation mechanisms mediated by the heme.[76] Clearly, the spin multiplicity of iron porphyrins is a property of fundamental interest which, as we shall see, still poses a challenge to electronic structure methods.

Investigation of heme systems using first-principles approaches, specifically Hartree–Fock (HF) and density functional theory (DFT), yielded reasonable results for structural parameters, and greatly contributed to the interpretation and understanding of the functional aspects of the active site of hemoproteins at the molecular level, as will be shown in the following sections. However, attempts to predict the ground state multiplicity of these systems soon made it apparent that an accurate description of the spin state might require more sophisticated techniques. This fact can be tracked down to the spin-transition energies provided by HF and DFT for isolated iron atoms and ions or different iron compounds, where it has been systematically observed that HF favors high-spin electronic configurations while DFT exhibits a preference for low-spin states.[75,77] For example, for the ground states of the series $Fe^0/Fe^+/Fe^{2+}/Fe^{3+}$, experimentally high-spin, HF always overestimates the quintuplet–triplet (or sextet–quartet) splittings with errors going from 1.5 to 35 kcal mol^{-1}.[75] DFT, on the other hand, underestimates the same transition energies by 5–35 kcal mol^{-1}, predicting for the case of Fe^+ a triplet instead of a quintuplet.[75] Such biases in HF and DFT are similarly manifested in heme complexes. Table 1 summarizes this trend as observed in five- and six-coordinated models of the heme group.

For the last decade DFT has been the first method of choice to perform electronic structure calculations of biological models, and in particular of heme systems. In this context, one of the most embarrassing failures of DFT has been detected in the deoxygenated active site of hemoglobin and myoglobin

Table 1 Experimental and calculated electronic ground states of the active site of hemoglobin and myoglobin: iron(II) heme coordinated to imidazole (five-coordinated) and to imidazole plus O_2 (six-coordinated)

	Six-coordinated	Five-coordinated
Experimental	Singlet	Quintuplet
Hartree–Fock	Quintuplet	Quintuplet
DFT-GGA	Singlet	Triplet
B3LYP	Singlet	Triplet

(Table 1). The earliest study reporting this flaw of DFT is due to Rovira *et al.*,[74] who obtained for the five-coordinated heme (axial ligand: imidazole) a triplet state 6.5 kcal mol^{-1} below the quintuplet, the experimental ground state of the system. After this work, a few others followed which also found this inversion using B3LYP or different pure generalized gradient approximation (GGA) functionals.[75,78] Interestingly, it was shown that the relative ordering of multiplicities is very sensitive to the out of plane displacement of the iron atom, $d_{Fe\text{-}p}$. At a value of $d_{Fe\text{-}p}$ close to 0.4 Å, DFT leads to a spin crossover which leaves the potential energy surface of the quintuplet below, restoring the correct order of spin states.[74,78] Liao and Scheiner, using pure DFT, claimed to have found a quintuplet ground state for the deoxy-, five-coordinated heme.[79] In their calculations, however, electronic symmetry constraints were imposed. To the best of our knowledge, DFT functionals yield for this complex a triplet ground state in the absence of symmetry constraints.

Ghosh and Taylor resorted to highly-correlated techniques as CASPT2 and CCSD(T) to quantify the errors in the DFT estimates of spin transition energies in iron porphyrins.[77] These authors examined the iron(III) porphyrin chloride, another example of a high spin five coordinated heme complex for which DFT predicts a quartet favored over the sextet, in this case by around 7 kcal mol^{-1}. B3LYP, on the other hand, finds about the same energy for both spin configurations. The more accurate approaches CASPT2 and CCSD(T) agree in yielding a sextet ground state, 16 kcal mol^{-1} below the quartet.[77] Yet, beyond these specific examples involving high-spin complexes, it would be unfair to misjudge DFT and forget its many successes in evaluating energies and structures of heme species of low and intermediate multiplicity. DFT is still applied in many cases in which the system is known experimentally to be high-spin, adopting the experimental multiplicity for the calculation, even if it does not correspond to the lowest energy state according to the method. Care must be taken with this practice since, even though useful for some applications, it will provide significantly biased energetics for processes involving spin transitions. Thus, computed binding energies (*e.g.* to O_2 or other diatomic ligands) will be likely too large, because the total energy of the reactant, high spin, will be overestimated with respect to that of the product, low spin.

The errors committed by DFT or HF are related to the balance between the computed electronic exchange and correlation energies. In a simplified picture, the (negative) exchange energy is contributed by like spin electron pairs, whilst electronic correlation arises from the interaction between electrons

regardless of their spin. A method which considers only the exchange, as HF does, will favor high multiplicities by maximizing the number of electrons with the same spin. To the contrary, experience shows that the combination of the exchange and the correlation terms in pure DFT pushes the balance toward low spin configurations.[80] Attempts to improve the spin state energetics description of density functionals have mostly been based on hybrid Hartree–Fock/DFT schemes,[75,80,81] which combine the exchange of HF with the exchange and correlation obtained from DFT in proportions obeying empirical considerations. This approach, however, has given no universal functional capable of providing accurate splittings in every case. In general, those functionals offering a good description of the high spin species fail when tried out on low spin complexes, and *vice versa*.[75] Among them, B3LYP is seemingly the one with the best average performance up to now, yet producing serious inaccuracies in the five-coordinated models already discussed. An alternative approach to hybrid functionals, which might become a good compromise between cost and accuracy, is a recent implementation of the LDA + U or GGA + U method originally designed for the treatment of strongly correlated materials.[82] This approach intends to improve the correlation energy by introducing a correction on the orbital energies based on the linear response of the system. Very recent calculations have proven it successful in the estimation of spin transition energies of small iron species.[83] Work on the suitability of this technique for the prediction of the spin state energetics of five- and six-coordinate heme models is underway.[84]

4. Interaction of heme proteins with small ligands: structure and energetics

The function of a large number of heme proteins involves the sensing, transport, and storage of diatomic ligands, such as O_2, NO and CO. This is achieved by the interaction of the heme group with these ligands, subtly modulated by the protein environment. Theoretical calculations have yielded relevant information about the equilibrium geometries and electronic structure of iron–porphyrin complexes. In particular, calculations performed on isolated Fe–porphyrin model systems in vacuum allow for a direct comparison with experimental structural data and help us understand the trends and correlations between the structure and chemical reactivity of the isolated heme group. The application of QM-MM schemes is especially useful for providing information about the structure of a protein–ligand complex, which may be unavailable experimentally. The relevant structural parameters of the heme–ligand complex in myoglobin, are shown in Fig. 2.

The characterization of the ligand affinity of heme proteins and porphyrin models has been the subject of many studies in the last decades. The main experimental parameters related to ligand affinity are the association (k_{on}) and dissociation (k_{off}) rate constants for ligand binding corresponding to the following reactions:

$$\mathrm{FeP} + \mathrm{L} \rightarrow \mathrm{FeP\text{-}L}(k_{on}) \quad \text{and} \quad \mathrm{FeP\text{-}L} \rightarrow \mathrm{FeP} + \mathrm{L}(k_{off})$$

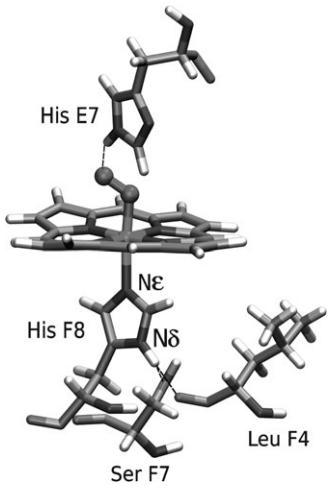

Fig. 2 Representation of the heme–O_2 complex in myoglobin, showing also the more relevant amino acids close to the active site.

The affinity or equilibrium constant (K_{eq}) can then be obtained from these kinetic constants, or from equilibrium measurements. The ligand association process, characterized by k_{on}, is mainly related to the ligand migration across the protein, as discussed in section 2. On the other hand, the process of ligand release is controlled by the Fe–L bond breaking and is therefore intimately related to the calculated ΔE for ligand dissociation. Computational simulation complements structural and dynamical insights from heme–ligand chemistry obtained from spectroscopic studies, in particular from resonance Raman and IR studies of the heme–ligand complexes.[85]

In this section we will present results concerning binding of O_2, NO, HNO and CO to heme proteins. In each case, a brief comparison of the results obtained with different methods for the isolated complexes is included. Also, selected examples of QM-MM calculations of binding energies in heme proteins are reviewed. The results contributed by our group correspond to simulations performed using the SIESTA electronic structure scheme,[86] based on DFT. In this implementation, the electronic wave function is expanded in localized (numerical) basis functions projected on a real space grid, in combination with norm-conserving pseudopotentials to represent the nuclei and core electrons. Double zeta plus polarization basis sets were employed, with a pseudoatomic orbital energy shift of 25 meV and a grid cutoff of 150 Ry.[86] Calculations were performed using the generalized gradient approximation functional proposed by Perdew, Burke and Ernzerhof (PBE).[87] Hybrid QM-MM calculations were performed using our own QM-MM implementation on the SIESTA code,[88] treating the QM subsystem at the DFT level as described above, whereas the classical region is described using the Amber99 force field parametrization.[89] In all the cases mentioned in this section, the heme group, the exogen ligand and the imidazole ring of the proximal histidine conform the QM subsystem. The rest of the protein was treated classically. The frontier between the QM and the MM subsystems was treated with the link atom method.[88]

Table 2 Selected structural (Å and °) and energetic parameters (kcal mol^{-1}) for the porphyrin Fe(II) oxygen complex

	SIESTA[90]	Car–Parrinello[74]	Expt.[91]
d Fe–O	1.77	1.77	1.75
d O–O	1.29	1.30	1.16
∠ Fe–O–O	121.8	121.0	131
d Fe–Nδ (His)	2.12	2.08	2.07
ΔE	22.2	15.0	—

4.1 The heme–O_2 complex

Most heme proteins interacting with oxygen display a histidine residue as the proximal ligand. We will focus our discussion on these cases.

Structure of the heme-O_2 complex. Table 2 shows relevant structural (angstroms and degrees) and energetic (kcal mol^{-1}) parameters for an isolated imidazole–porphyrin (Fe^{II})–O_2 complex as obtained with two different DFT implementations: the SIESTA program using the PBE exchange–correlation functional, and the Car–Parrinello scheme using the BLYP functional. Experimental values are also shown.

A good agreement between the calculated geometrical parameters and the experimental values is observed. The optimized Fe–His bond distance in the pentacoordinated complex is 2.22 Å. Upon oxygen binding, the DFT calculations at the SIESTA level predict a shortening in the Fe–His bond distance of about 0.1 Å, the so called positive *trans* effect.

The structure of the oxy complex in heme proteins displays small deviations from the isolated complex due to the interactions between the prosthetic group and its environment. The protein control on heme ligand chemistry may be classified in distal and proximal effects as they are produced by residues located in the distal and proximal sides of the heme plane, respectively.

Distal effects. Distal H-bond donor residues are found in most oxygen binding heme proteins, in most cases increasing heme protein's affinity for this ligand. Due to the effect of π–backdonation from the iron to the O_2, the ligand becomes negatively charged and is therefore a good H-bond acceptor. Typical distal residues available for H-bonding are tyrosine, histidine, and glutamine. More than one distal residue capable of interacting may be present in the active site, generally increasing the affinity. Table 3 shows relevant structural parameters for the oxy complexes of two heme proteins calculated by our group with the SIESTA code: (i) truncated hemoglobin N (trHbN), which displays two H-bond donor residues, Tyr33 and Gln58, in the distal side; (ii) myoglobin (Mb), which has a distal histidine residue.

Table 3 Geometrical parameters (Å and °), charge received by the O_2 (ΔqO_2) and donated from the proximal histidine to the Fe (Δq_{prox}) (in *e*), and O_2 affinity (kcal mol^{-1}) for the active sites of TrHbN and Mb

	trHb N[92]	w.t. Mb[90]
d Fe–O	1.84	1.84
d O–O	1.31	1.30
< Fe–O–O	120.7	120.9
d Fe–Nδ (His)	2.06	2.18
ΔqO_2	−0.360	−0.214
Δq_{prox}	0.160	0.146
ΔE	37.2	27.7

As can be seen from Table 3, differences for the structural parameters between these proteins are small. The results for the O_2 binding energy confirm the stronger distal stabilization in TrHbN with respect to Mb. H-Bond interactions are also found to increase the oxygen negative charge. The modulation of O_2 affinity is therefore achieved through direct H-bonding and increased π–backbonding, resulting in a higher binding energy to the oxygen molecule.

Proximal effects. As pointed out in the last section, distal effects are able to determine in a drastic way the O_2 affinity of a heme protein. Similarly, the influence of the proximal histidine and its environment cannot be neglected. An investigation of proximal regulation recently reported by our group[90] proposed three different factors intervening in proximal regulation: first, the charge donated from the proximal histidine to the Fe atom (charge relay mechanism); second, the proximal histidine rotational position; and third, the Fe–His distance.

When the charge donated by the proximal histidine to the Fe atom is changed we have the first effect, which will cause the variation of O_2 affinity. The charge donated by the proximal histidine is closely related to H-bond interactions of this histidine with the protein side chains. Our computational results suggest that there is a certain degree of charge donation which maximizes the affinity, and is obtained through an H-bond with the oxygen atom of a carbonyl group, as found in many O_2 transport heme proteins.

The second effect is related to the histidine rotational position, which is defined as the dihedral angle formed by the imidazole plane and the line that goes through two opposite pyrrolic nitrogen atoms of the heme group (see Fig. 3). When this angle is close to 45°, the geometry is called staggered, and when it is close to 90° it is called eclipsed, being the first one the most favorable for O_2 binding.

The last effect corresponds to constraints in the Fe–Nε distance. Our results show that when this distance is reduced, the O_2 binding energy increases.

An example of proximal regulation is found in leghemoglobin (Lba). It has been shown that, at variance with Mb, in Lba there is not an important distal stabilization effect. Even so, O_2 affinity is slightly larger in Lba than in Mb. The molecular basis of proximal regulation in this protein has been investigated by means of QM-MM calculations on w.t. Lba and

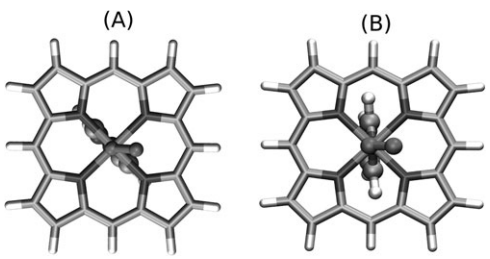

Fig. 3 Histidine rotational position: (a) eclipsed; (b) staggered.

selected mutants, showing that proximal effects are responsible for the observed affinity.[90]

4.2 The heme–CO complex

The structural and energetic properties of the Fe–CO moiety in porphyrins and heme–proteins are of special interest and have been the subject of numerous studies.

Structure of the Fe–CO complex. In contrast to what is observed in the Fe–O_2 complex, the FeCO angle is normally close to 180° as a consequence of the symmetry of the molecular orbitals involved in the bond, since the backbonding between Fe d_π orbitals with the π^* orbitals of CO is maximized at a linear conformation. DFT calculations on a porphyrin model (iron–porphyrin-CO) showed that the adduct is a closed shell singlet with a binding energy of 26 and 33 kcal mol^{-1} according to the Car–Parrinello method at the DFT-BP86 level,[74] and to the SIESTA method at the DFT-PBE level, respectively. The Mulliken charges on the C and the O atoms do not change significantly with respect to the isolated CO. The incorporation of imidazole as sixth ligand increases the binding energy to 35 kcal mol^{-1}.[74] This strengthening can be understood in terms of orbital interactions, since the inclusion of imidazole induces a better overlap between the Fe-d_{z2} and the CO-σ orbitals.[74]

The results from most theoretical and experimental works confirm that carbon monoxide binds linearly to the iron. Some early works based on X-ray claimed that the angle of the Fe–CO unit was distorted in some heme–proteins, suggesting a possible mechanism for CO/O_2 discrimination by steric hindrance.[94] Calculations on this issue showed that the energetic cost for small tilting and bending distortions of the Fe–CO angle are very small (*e.g.* 2 kcal mol^{-1} for 25°).[95,96] Vangberg estimated a barrier of less than 1 kcal mol^{-1} for a 7° distortion, but found that deviations larger than 15° are prohibitive.[97] Additional calculations were performed by Rovira and coworkers to explore in more detail the shape of the potential energy surface, incorporating the sixth ligand to the system. Using molecular dynamics simulations and a QM/MM scheme, they reported a quite rigid Fe–CO bond, with little distortion around its equilibrium position, and inexpensive rotation of the imidazole ligand, in agreement with experiments.[93]

Vibrational characteristics of the CO unit as a molecular probe. The CO stretching frequency in the FeCO moiety has been used to monitor the structure and bonding in CO adducts. When CO binds to heme, its frequency diminishes approximately 200 cm^{-1} from the corresponding value in isolated CO, 2143 cm^{-1}. The exact frequency is sensitive to the backbonding, which in turn is modulated by the molecular environment of the bound CO. This property has been exploited using the CO frequency (ν_{CO}) as a vibrational probe in heme protein's active sites.[98,99] Several works[100,101] noted a negative correlation between ν_{Fe-CO} and ν_{CO}. Provided that the sixth ligand is unchanged, these two frequencies have been found to correlate linearly. Studies in which this effect is explored involved a variety of substituents in the porphine ring with different electron donating and withdrawing capacity, in order to alter the extent of backbonding in the proximal residue. Donating ligands *trans* to CO displace the correlation plot to steeper slopes and lower Fe–CO frequencies, reflecting the competition of the ligand lone pair for the σ acceptor orbital d_{z2}.[102] When CO is bound to a heme group in a heme protein, different ν_{CO} absorption bands are observed depending on temperature, pressure, pH or solvent. In Mb, four main infrared bands are identified, denoted A_0, A_1, A_3 and A_x, which relative intensities are modulated by the experimental conditions. Using a QM-MM approach to simulate Mb–CO, Rovira *et al.*[93] concluded that the ν_{CO} frequencies depend mainly on the position of the His64 amino acid (the distal residue), suggesting that the imidazole is protonated at N_ε.

4.3 The heme–NO complex

In contrast to O_2 and CO, both of them reactive towards the reduced (Fe^{II}) heme group only, nitric oxide (NO) is able to bind to the heme's iron in the reduced (Fe^{II}) and oxidized (Fe^{III}) states. The resulting nitrosyl complexes were classified by Enemark and Feltham on the basis of the number of electrons in the metal d orbitals plus the number of electrons in the π orbitals the NO, which is given by *n* in the $\{FeNO\}^n$ notation.[103,104] Therefore, the reaction between a ferric heme and a NO yields a $\{FeNO\}^6$ complex, whereas the NO reaction with a ferrous heme yields a $\{FeNO\}^7$ complex. These two types of complexes exhibit significant structural differences.

Structures of heme–NO complexes. Table 4 shows the relevant structural parameters for isolated heme–NO complexes calculated with different electronic structure schemes, together with experimental values obtained for hexacoordinated nitrosyl porphyrin complexes. For all cases the proximal axial ligand is an imidazole group.

As can be seen, DFT results are in good agreement with the experimental values. The main differences between the $\{FeNO\}^6$ and $\{FeNO\}^7$ complexes are in the Fe–NO geometry. The $\{FeNO\}^6$ complex is linear or nearly linear whereas the $\{FeNO\}^7$ is bent. In addition, Fe–N(NO) distances are longer in $\{FeNO\}^7$ than in $\{FeNO\}^6$. The $\{FeNO\}^6$ geometry

Table 4 Geometrical parameters of nitrosyl–heme complexes. Distances in Å, angles in °

	SIESTA-PBE		DFT-B3LYP[105]	Car-Parrinello[74]	Experimental[103,106]	
	$\{FeNO\}^6$	$\{FeNO\}^7$	$\{FeNO\}^6$	$\{FeNO\}^7$	$\{FeNO\}^6$	$\{FeNO\}^7$
d Fe–N (NO)	1.651	1.75	1.639	1.72	1.650	1.74
d N–O	1.165	1.18	1.136	1.20	1.130	1.12
∠ Fe–N–O	177.3	137.7	179.7	138	177.0	140
d Fe–Nε (His)	2.044	2.17	2.024	2.22	1.983	2.18

is similar to the one found in the isoelectronic $Fe^{II}CO$ complex. This fact and the high NO stretching frequencies observed (1917–1921 cm^{-1}),[103] suggested that the complex could be described formally as Fe^{II}–NO^+ instead of Fe^{III}–NO. The Mulliken population analysis supports the positive character of the NO. On the other hand, in the $\{FeNO\}^7$ system the NO displays a slightly negative charge. The electronic density of the NO is important as far as it determines the kind of interactions which will arise with the protein environment. Both types of NO complexes also differ significantly in their stability; while $\{FeNO\}^7$ complexes are not reactive and exhibit a very small dissociation constant ($k_{off} \approx 10^{-4}$ s^{-1}), the NO^+ character of the nitrosyl group in $\{FeNO\}^6$ complexes makes them susceptible to nucleophilic attack, and NO dissociation is relatively fast ($k_{off} \approx 10^3$ s^{-1}).[107]

Another important fact in nitrosyl complexes is the so called NO negative *trans* effect, consisting of weakening of the bond *trans* to the NO upon NO binding. This behavior is typically observed in the $\{FeNO\}^7$ complexes, producing the lengthening of the Fe–His bond in heme proteins upon NO binding.

Biological implications. The interaction of NO with heme proteins has been widely studied as it is involved in many important biological functions. Particularly interesting is the fact that nature has taken advantage of the two types of NO interaction with hemes.

The $\{FeNO\}^7$ complex in proteins. The most relevant example of a protein where the $\{FeNO\}^7$ complex plays a role is the soluble form of guanylate cyclase (sGC), the mammalian receptor for NO. In this protein, the formation of the 5c-NO complex, associated to the Fe–His bond breaking due to the negative NO *trans* effect, is considered to trigger a conformational change that activates the enzyme and transduces the NO signal.[108] Since the structure of sGC is unknown, many studies aimed to get a better understanding of the molecular mechanism responsible for sGC activation relying on the study of NO interaction with other histidine coordinated ferrous heme proteins. In particular, attention has been addressed to the modulation of the NO *trans* effect. The proximal His–Fe bond is not broken upon NO binding in all heme proteins. Therefore, heme proteins could be classified in two groups, one including those retaining an iron–histidine bond in the Fe^{II}–NO complex, and one with those in which the Fe–His bond is broken. Experimentally, it was initially observed that those proteins with a strong Fe–His bond, evidenced by high Fe–N(His) stretching frequencies (>210 cm^{-1}), would maintain the Fe–His bond upon NO binding.[109] Our theoretical work showed that an important issue regulating the Fe–His bond strength and thereby the breaking process, is the charge density of the histidine's imidazole ring, which is dependent on H-bond interactions between the Hδ atoms of the histidine with surrounding residues (charge relay mechanism). Strong H-bond interactions, formed for example with a carbonyl or carboxylate group, inject charge into the conjugated ring thus strengthening the histidine–iron bond, which would not dissociate in the Fe^{II}–NO complex. Recently new evidence challenged this hypothesis, due to the finding of two proteins where the bond is broken upon NO binding although they display high Fe–N(His) stretching frequencies (231 cm^{-1} and 220 cm^{-1}).[110,111] In particular, one of these two proteins, cytochrome c′ (Cyt c′),[110] is found in the periplasm of certain bacteria and shares spectroscopic and ligand binding characteristics with soluble guanylate cyclase (sGC). Kinetics studies on sGC suggested that NO is not only acting as an exogenous heme group ligand, but also catalyzes the transformation from the 6c-NO to the 5c-NO complex, by participating in the Fe–His bond breaking.[112,113] However, other studies performed by Bellamy *et al*. showed that it is not necessary to consider a second NO in this reaction.[114]

The hypothesis proposing the intervention of a second NO was later supported by more evidence coming from studies on Cyt c′. X-Ray crystallography on Cyt c′ from *Alcaligenes xylosoxidans* assigned the NO to the proximal site previously occupied by the histidine. This information suggested that the mechanism of 5c-NO complex formation could be more complicated than a simple Fe–His bond breaking induced by NO binding. QM-MM calculations on Cyt c′ showed that there is a local structural minimum corresponding to the Fe–His bond broken and the histidine interacting with an arginine residue located close to the proximal cavity. These results also showed that two different mechanisms for Fe–His bond breaking may exist with or without the catalytic action of a second NO molecule. The fact that NO is found coordinated to the Fe by the proximal side could be justified by *in silico* generated Cyt c′ mutant proteins. Simulations with these modified proteins showed that the existence of a leucine residue in the distal cavity produces sterical hindrance for NO binding in the distal side, and so the proximal side is preferred.[115]

The $\{FeNO\}^6$ complex in proteins. Nature has taken advantage of the fast NO dissociation in the $\{FeNO\}^6$ complexes (0.65 to 40 s^{-1}),[116] thereby allowing a heme protein to function as a NO carrier. This group of heme proteins acting as NO carriers, so called nitrophorins (nitro = NO, phorin = carrier) are able to store NO in the salivary glands of some bloodsucking insects, and then releasing it upon dilution and pH increase in the victim's blood.[117] Four nitrophorins (named NP1 to 4) were cloned and later crystallized from *Rhodnius prolixus*,[118,119] showing the typical linear Fe–NO unit characteristic of the $\{FeNO\}^6$ complexes. However, in some crystals of NP4 the authors observed also an unusual conformation in which the FeN(NO) and NO vectors were strongly tilted, but in opposite directions. The authors proposed that this orientation may correspond to a "loosely bound" or side-on bound NO. Wondimagegn and Ghosh[120] performed DFT based calculations on several porphyrin model systems in order to study the possible multiple FeNO conformations of the $\{FeNO\}^6$ complexes. These authors obtained a local minimum on the potential energy surface (1.34 eV higher in energy than the linear FeNO complex) corresponding to the so called out of phase tilted and bent structure for the $[Fe–porphyrin–imidazole–NO]^+$ complex, in agreement with the experimental observation in NP4. The authors also showed that in the five coordinated $\{FeNO\}^6$ complex (without the imidazole ligand) and all the $\{FeNO\}^7$ complexes this linkage isomer does not exist.[120] Whether this

Table 5 Selected geometrical parameters of heme–HNO complexes (Å and °). The first and the second columns correspond to SIESTA calculations using the PBE functional

	FePor–HNO	Mb–HNO (QM-MM)	Mb–HNO (expt.)[133]
d Fe–N_{por}	2.03	2.02	2.00
d Fe–N_{His}	2.10	2.17	2.09
d Fe–N_{NO}	1.79	1.78	1.82
d N–O	1.25	1.26	1.24
∠ Fe–N–O	131.7	132.3	131

tilted and bent structure is relevant for the protein's function remains to be proven.

4.4 The heme–HNO complex

In the last years there has been an increasing interest in the one-electron reduction product of NO, nitroxyl (HNO). It has been reported that HNO can be produced under certain conditions by nitric oxide synthase,[121–123] and that nitric oxide (NO) and nitroxyl (HNO/NO^-) donors may exhibit distinct pharmacological effects.[124–128] Since the most relevant molecular targets of HNO are heme proteins,[129–132] understanding their interaction is of primary concern in HNO biochemistry. HNO readily reacts with ferric heme proteins yielding the same Fe^{II}–NO complex obtained by the reaction of ferrous heme protein with NO. HNO has also been shown to react with Fe^{II}Mb yielding the Mb–HNO adduct.[133] Table 5 shows the structural parameters resulting from calculations on an isolated HNO–porphyrin, on a HNO–myoglobin structure, and the parameters from X-ray absorption data for HNO-Mb.[133]

As can be seen from Table 5, the results obtained in the QM-MM calculation are in agreement with the experimental data. The calculated HNO binding energies are 53.2 and 55.9 kcal mol^{-1} for an isolated porphyrin and Mb, respectively. This means that the protein stabilization is small. However, an increase of 2–3 kcal mol^{-1} in the binding energy would represent a $\sim$100 times lower dissociation rate constant in the protein compared to a free porphyrin in organic solvent. An interesting issue about HNO complexes is whether or not they display a negative *trans* effect. The computed Fe–His bond distances in the HNO porphyrin and the free heme are 2.10 and 2.16 Å, respectively, suggesting that there is no negative *trans* effect in this case. However, if the complex is deprotonated the resulting $\{FeNO\}^8$ species displays an enhanced negative trans effect, with a computed Fe–His bond distance of 2.39 Å.

5. Chemical reactivity of heme proteins

Besides sensing and transport of small ligands, heme proteins are also responsible for the catalysis of a variety of chemical reactions, including the oxidation of organic molecules, NO detoxification, nitrite reduction to NO, *etc*. Computer simulation experiments, specifically QM calculations on model systems and QM-MM studies, have been successfully employed to shed light on the molecular basis of the catalysis. In this section we will present several representative examples that cover both approaches.

5.1. NO scavenging by oxygenated heme proteins

The toxic effects of NO can be reduced or even eliminated by the development of resistance mechanisms, typically consisting in the oxidation of nitric oxide by the O_2 bound to heme to yield the innocuous nitrate ion:

$$Fe(II)O_2 + NO \rightarrow Fe(III) + NO_3^- \qquad (1)$$

NO scavenging functions have been observed in red blood cell hemoglobin, muscle myoglobin, neuroglobin within neuronal cells, and leghemoglobin, as well as in flavohemoglobins and truncated hemoglobins.[134]

The heme-controlled oxidation of NO in *M. tuberculosis* truncated hemoglobin N (trHbN) has been investigated by our group using QM-MM calculations.[92] The optimizations in trHbN placed the NO molecule in the active site close to O_2 interacting with Tyr33 and Gln58 residues (Fig. 4). The oxidation reaction of NO was examined considering a mechanism in which a peroxynitrite ion is formed from the attack of NO to the coordinated O_2, with a subsequent isomerization in two steps of peroxynitrite to nitrate mediated by the metal center:

$$Fe(II) - O_2 + NO \rightarrow Fe(III)[^-OONO] \qquad (2)$$

$$Fe(III)[^-OONO] \rightarrow Fe(IV) = O + NO_2 \qquad (3)$$

$$Fe(IV) = O + NO_2 \rightarrow Fe(III)[NO_3^-] \qquad (4)$$

Calculations were performed for four models: (i) the isolated system in vacuum; (ii) the same system in an aqueous solution (using a cluster of 1061 water molecules); (iii) the wt protein; and (iv) the Tyr33 → Phe mutant.

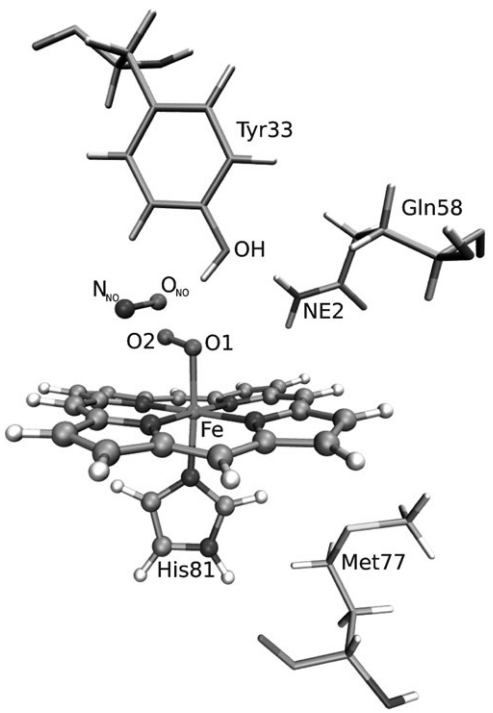

Fig. 4 Representation of the trHbN active site.

The results derived from QM-MM calculations indicate that the protein catalyzes the chemical reactions leading to the formation of nitrate mainly by means of the heme group, with no significant contributions of the protein environment, suggesting that the rate limiting process is ligand diffusion to the heme, as can be seen from the experimental bimolecular rate constant (745 μM^{-1} s^{-1})[44] typical of a diffusion controlled process. The same process in myoglobin has also been investigated by means of B3LYP calculations in model systems. The barrier going from the oxy-Mb and NO to form the peroxynitrite intermediate was found to be around 10 kcal mol^{-1}, while the barrier to form the oxo-ferryl and NO_2 radicals (step 3) was of about 7 kcal mol^{-1}. The overall process was found to be exergonic by more than 30 kcal mol^{-1}.[135]

5.2 Hydroxylation reaction catalyzed by Cytochrome P450

Cytochrome P450 enzymes (P450) are the most important members of the heme–thiolate proteins family, characterized for containing in their active site an iron porphyrin connected to the protein through an iron–cysteinate bond.[136–141] P450s are present in most organisms (mammals, fish, invertebrates, plants, and microorganisms), and catalyze a large variety of reactions, such as oxidation, reduction, isomerization, and dehydration processes. These reactions are important for the biodegradation of toxic substances, as well as for biosynthesis (*e.g.* sex hormones). As such, P450 enzymes are vital, drawing a soaring interest aimed at understanding of their nature and reactivity patterns. They activate dioxygen and carry out mono-oxygenation in a variety of endogenous and xenobiotic compounds. The importance of these processes for life has presented an exciting agenda for research aimed at the elucidation of the mono-oxygenation mechanisms and the identification of the intermediate species in the catalytic cycle of the enzyme.[141] Important insights into the nature of the enzymatic cycle resulted from computational studies of various isozymes as well as of synthetic model metalloporphyrins in different oxidation states and with various ligands.[142,143] The most extensive research efforts were devoted to the hydroxylation of alkanes and the epoxidation of alkenes.[67,144–159]

The commonly accepted catalytic cycle for P450 is shown in Scheme 4.[140,141] The consensus rebound mechanism,[148] suggested by Groves *et al.*,[151,152,160] corresponds to reactions from species **2** to **4**. This involves initial hydrogen abstraction from the alkane (R-H) by the active ferryloxene species (**2**, $Por^{\bullet+}Fe^{IV}$-O, Por = porphyrin), known also as Compound I,[148,161–166] followed by radical rebound on the ferryl-hydroxo intermediate, **3**, to generate the ferric-alcohol complex **4**. While the intermediacy of the precursor hydroperoxy complex **1** has recently been ascertained by electron nuclear double resonance (ENDOR) spectroscopy under turnover conditions,[150] compound I (**2**) remains elusive and the mechanism of hydroxylation is still controversial.

The electronic structure of **2** has been widely discussed in the literature by several groups,[67,154–156] based on isolated gas phase QM characterizations, UV-VIS spectra calculations, and QM-MM simulations in the active site of the P450cam enzyme.

Significant contributions to the understanding of the catalytic activity of this enzyme are due to Shaik and Thiel's groups.[157,162–171] These works cover a wide range of computational calculations, from the study of the epoxidation reaction of ethene by species **1**[170] and **2**[169] in isolated model systems, to the alkane hydroxylation by **2** in both vacuum[168] and in the P450cam active site.[171] Guallar and Friesner also contributed to elucidate this issue using several methodologies from vacuum calculations to hybrid QM-MM schemes and

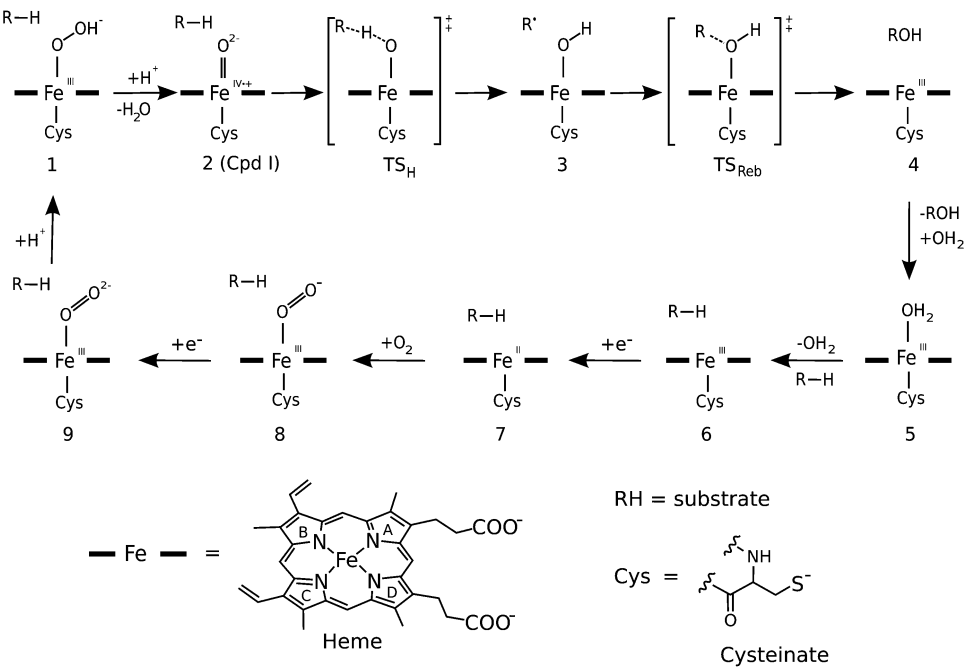

Scheme 4 Schematic representation of the catalytic cycle of P450 enzyme and the rebound mechanism. The cycle starts in the resting species with water coordinated to ferric-heme (5).

molecular dynamics simulations.[172–175] In particular, the authors centered their efforts in the role of the protein in the steps of protonation and reduction of ferric-superoxo (**9**) to ferric-hydroperoxo (**1**) and the substrate hydroxylation by the rebound mechanism.

The epoxidation pathways of ethene by a model for Compound I (**2**) of cytochrome P450[169] and by its precursor, $[PorFe^{III}–OOH]^-$ (**1**),[170] recently identified by EPR/ENDOR spectroscopies,[150] have been studied with DFT calculations. Four epoxidation pathways of **1** were located with barriers of 37–53 kcal mol^{-1}, in comparison with 14 kcal mol^{-1} for epoxidation by Compound I, concluding that $[PorFe^{III}–OOH]^-$ (**1**) cannot be a second oxidant, and suggesting that P450 uses a single oxidant, Compound I (**2**).

The protonation of the ferric-superoxo (**9**) was investigated using a quantum model and molecular mechanics simulation in the P450eryF enzyme[174] and QM-MM methodologies in the P450cam enzyme.[175] The authors have shown the need to have a reduced, low-spin ferric superoxo (**9**) prior to proton addition, and the importance of a chain of hydrogen bonds in a water channel involving at least two water molecules and the residues Ser246 (in P450eryF) and Tre252 (in P450cam). Under these conditions a fast protonation step may occur, and in fact molecular dynamic simulations indicated that the conformations required for this fast protonation are visited with enough frequency.

DFT has also been applied to study the rebound mechanism of alkane hydroxylation in a model of the active site of the enzyme cytochrome P450.[168] The results corroborate the Groves's rebound mechanism[142] and highlight a key feature: the reactivity patterns and product distribution result from the interplay of two reactive states of the active compound I species (**2**) of the enzyme: the low-spin (doublet) and the high-spin (quartet) states.

Another interesting example investigated with QM-MM approaches is the stereospecific cytochrome P450-catalyzed hydroxylation of the $C^5–H^{5\text{-exo}}$ bond in camphor.[171,175,176] Kamachi and Yoshizawa[176] obtained an activation energy of 23 kcal mol^{-1} to produce the first transition state through hydrogen atom abstraction, concluding that this should be the rate-determining reaction because the rebound step connecting **3** and **4** is virtually barrierless in both spin states. Moreover, the conversion of the iron-peroxo species (**1**) to compound I (**2**) is exothermic by 50 kcal mol^{-1}, probably being the driving force in alkane hydroxylation by cytochrome P450.

Shaik and Thiel[171] calculated the energy profile of the hydrogen-abstraction oxygen-rebound mechanism, obtaining an activation energy for the hydrogen-abstraction reaction approximately 20 kcal mol^{-1} in both spin states, while for the rebound step it is only 3 kcal mol^{-1} for the high-spin species and barrierless in the doublet surface. They have also assessed the effects of the heme-propionate side chains, including residues Arg299 and Arg112 in the simulation, which form a salt bridge with them. They concluded that propionates, which are electrostatically screened by the Arg residues, carry no spin density, neither in the enzyme nor in the gas phase, and therefore there is no significant charge transfer from the propionates to the porphyrin or to the thiolate ligand. Guallar and Friesner[175] investigated the role of the protein in the energetics of this reaction and found it endothermic by 4.5 kcal mol^{-1}. Furthermore, they concluded that the protein has a fundamental role in this fast reaction by stabilizing the products (**4**) and transition state structures ($\mathbf{TS_H}$) and destabilizing the reactant (**2**), due to an electrostatic interaction between the propionate chains and the positive residues in close contact with them.[176] The discrepancies in relative energies, spin densities, and the role of the propionates obtained by Shaik and Thiel[171] on one side and Guallar and Friesner[173,175] on the other has recently been analyzed by these authors,[177] concluding that those discrepancies were due to the choice of the initial structures (taken from MD and X-ray data in the works of Shaik and Thiel, and Guallar and Friesner, respectively) and to technical details in the optimization procedures.

We have seen that the catalytic activity of cytochrome P450 enzyme has been widely studied by means of computational methodologies. The preceding results corroborate the rebound mechanism and show that the active hydroxylating species is compound I (**2**), and that the process involves a two-state reactivity scenario, whereby reactivity patterns and product distribution are determined by the interplay of two spin states.

5.3 Nitrite reduction processes

Nitrite reductases (NIRs) are a widespread class of enzymes which perform integral steps in the biochemical cycling of nitrogen. In the natural nitrogen cycle, nitrite (NO_2^-) is reduced by two types of NIRs. In the dissimilatory reduction, also called denitrification, NO_2^- is used as a respiratory terminal substrate. Two types of nitrite reductases have been found to be involved in this process, a copper protein,[178] and the heme protein Cyt *cd1*.[179] These NIRs catalyze the reduction of NO_2^- to NO:

$$NO_2^- + 1e^- + 2H^+ \rightarrow NO + H_2O \qquad (5)$$

On the other hand, it has been found that NAD(P)H-nitrite reductase, ferredoxin-nitrite reductase and Cyt *c* nitrite reductase, also known as assimilatory nitrite reductase, catalyze the reduction of NO_2^- to ammonia which is mainly used in the synthesis of amino acids:

$$NO_2^- + 6e^- + 8H^+ \rightarrow NH_4^+ + 2H_2O \qquad (6)$$

NIRs containing hemes *c* and *d*1 have been isolated from a large number of bacteria. Common source organisms include *Pseudomonas aeruginosa (Pa), Thiobacillus denitrificans, (Ps), Stutzeri, Ps. Halodenitrificans, Alcaligenes faecalis, and Paracoccus pantotrophus* (*Pp*).[180]

Over the last decade, contributions by Reutov[181] have underscored that deoxy hemoglobin and myoglobin have nitrite reductase activity, with the capability to generate NO. It has been suggested that the reaction of nitrite with deoxy–Hb may represent a significant source of NO bioactivity and may be the anaerobic counterpart of the oxygen dependent production of NO by nitric oxide synthase NOS.[182] It is tempting to speculate, then, that nitrite–deoxyheme protein interactions serve a more general role in tissue oxygen sensing.

Dissimilatory reduction of nitrite. The proposed reaction mechanism involves the following steps (see Scheme 5): nitrite

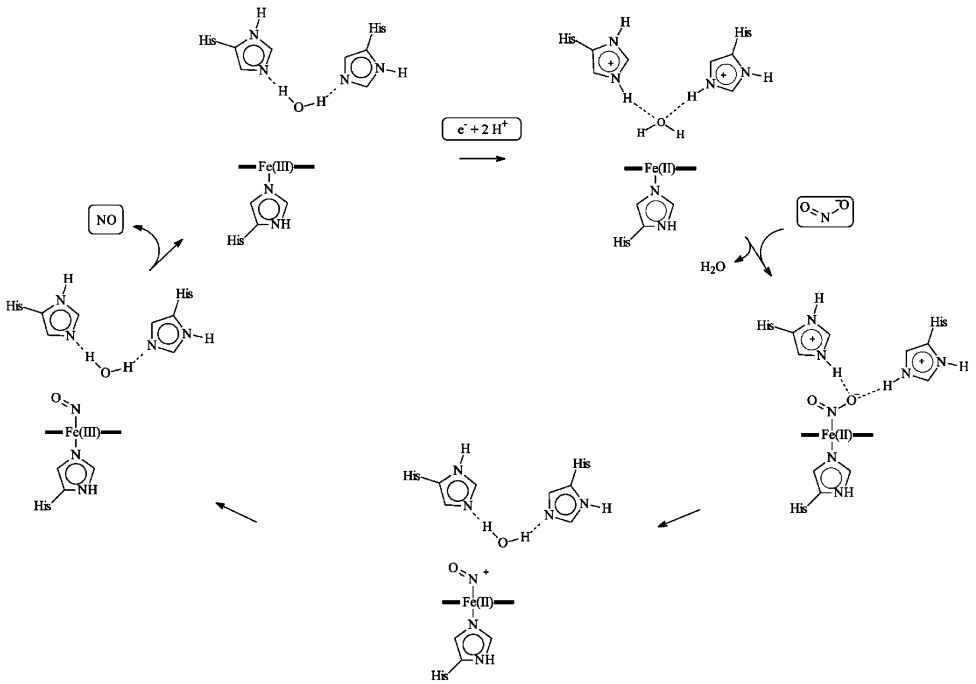

Scheme 5 Proposed reaction scheme for nitrite reduction by NIRs.

coordination to the reduced c*d1* heme, the formation of an $Fe^{II}(NO^{+})$ or an $Fe^{III}(NO)$ species[183] (denoted $\{FeNO\}^6$ in the Enemark and Felthan notation),[104] dehydration, subsequent release of NO, and an intramolecular electron transfer to regenerate the active site.

Common features in all reported bacteria NIRs are the presence of two invariant histidines and a tyrosine residue (His345, His388, and Tyr25 in *Pp*; and His327, His369, and Tyr10 in *Pa*), in the heme distal cavity. These histidines are ideally located to provide the protons required by the reaction and participate in a highly ordered array of hydrogen bounded water molecules. While both histidines have been found to be relevant for nitrite reductase activity,[184] Tyr does not seem to play a key role in catalysis.

Two theoretical investigations have been done on bacteria NIRs, one by Ranghino *et al.*[185] on *Pp*, and the other by our group on *Pa*.[186]

Ranghino *et al.* used a striped down model system of the active site of *Pp* NIR. The *ab initio* quantum mechanical model was then incorporated into the whole protein to account for the effect of charges elsewhere and the effect of screening and solvation, both by the protein and its immediate solvent environment. Structural minimizations, optimizations, and molecular dynamics calculations were performed on this system. Their results showed the feasibility of a concerted reaction path for the dehydration process in which one of the nitrite oxygen atoms binds to both protons of the protonated distal histidines in one step, leading to the $\{FeNO\}^6$ species. They also suggested that the NO releasing step could be assisted by a tyrosine and favored by unprotonated histidines.

The *Pa* NIR was investigated by us using QM-MM methods. Our results agree with those obtained on the model system for *Pp* NIR in the following aspects: the histidine stabilized by a nearby aspartic acid (His369 in *Pa* and His388 in *Pp*) is more likely to be protonated than the other, and nitrite binding affinity is greatly enhanced when both histidines are protonated. The QM-MM calculations suggest that the resting reduced state of the enzyme is probably monoprotonated in His327, and nitrite binding is thermodynamically favored in the mono- or bi-protonated active site. It has also been found that once nitrite is bound the proton affinity of the second histidine increases by more than 60 kcal mol^{-1}, and that the dehydration reaction occurs with a very low barrier, less than 2.4 kcal mol, either in a concerted or a two step mechanism. The Fe(III) metal center is finally reduced by internal electron transfer, leaving a water molecule or hydroxide ion coordinated to the Fe(II). Given the poor affinity of Fe(II) for water or OH^{-}, the ligand can be easily released, leaving the free enzyme ready for a new cycle. Since the involved proton transfers exhibit low barriers, these results suggest that the NO displacement is the limiting step of the whole reaction.

5.4 Degradation of heme by heme-oxygenase

Heme oxygenase (HO) is distributed in a wide variety of organisms such as bacteria, plants, and mammals, and its major function is freeing iron from heme for reuse (iron homeostasis). This enzyme proceeds by regioselective oxidation of the porphyrin ring at the α-position to produce biliverdin, carbon monoxide and free iron, using O_2 and NADPH. In this case, the porphyrin is the substrate instead of the prosthetic group. The crystal structure of HO revealed that the heme is incorporated into its active center between two helices. His25 in the proximal helix coordinates to heme as an axial ligand, while the steric influence of the distal helix permits the regioselective oxygenation at the α-*meso* carbon. The active species of the enzyme is the ferric hydroperoxide, Cpd 0, formed upon dioxygen uptake, followed by two-

electron reduction and protonation. Cpd 0 gives the α-*meso*-hydroxyheme, the competent reaction intermediate leading to biliverdin. Two possible mechanisms for the hydroxylation of the *meso* carbon atom had been proposed. The first one involves homolytic O–O bond dissociation of Cpd 0, followed by $OH^{\bullet}$ attack at the *meso* carbon atom, while the second one is an acid-catalyzed concerted electrophilic attack of the OOH moiety on the *meso* carbon atom, that is, a formal "OH^{+}" transfer. However, the free $OH^{\bullet}$ radical would be expected to attack the heme in a nonselective manner, and there are no specific acid or basic residues close enough to the FeOOH moiety to take part directly in the reaction. This reaction has been computationally investigated by two groups by means of DFT calculations on model systems at the B3LYP level.[187,188] Both research groups reported that the concerted transfer of the OH moiety to the α-*meso* carbon was found to proceed with an importantly high barrier of 40–46 kcal mol^{-1} due to a severe heme deformation at the transition state. Sharma *et al.* also found an acid-catalyzed and a non-acid-mediated stepwise mechanism with lower activation barriers of 20–26 kcal mol^{-1}. However, these works leave remaining some questions open, for example, if the reaction is proton assisted. A mechanistic study shows solvent kinetic isotope effect (KIE) and C_{meso}-D KIE which point to a proton-catalyzed mechanism.[189] It is still not clear whether the homolytic reaction is compatible with a regioselective hydroxylation of the α-*meso* carbon. There would not be an impediment for this if the enzyme surroundings of the heme pocket direct the preferred site for hydroxylation. This last issue may be settled by means of QM-MM calculations.

5.5 Electric field effects on heme

Many biological reactions in which heme proteins are involved take place in the proximity of lipid bilayer membranes where the presence of electric fields may affect the reactivity. In addition, changes in the local field originating in the electrostatic environment of a protein may also influence the active site reactivity. Several experimental and theoretical investigations have addressed this issue in the last years.

Electric fields can induce vibrational frequency shifts of reporter functional groups bound to heme which can be measured by infrared or Raman spectroscopy.[190] By computationally calibrating the vibrational Stark effect of these reporters, the magnitudes of the local field can be estimated. Vibrational Stark effects for the reporters CO, NO and CN bound to heme have been determined by DFT calculations.[191] For the same reasons, there is also a considerable interest in the determination of the nuclear magnetic resonance chemical shifts induced by electric fields. Results of *ab initio* calculations agree well with observed correlations of ^{13}C and ^{17}O chemical shifts and CO vibrational frequencies in carbonmonoxy heme proteins.[192] The local electric field has also been estimated employing classical force fields by direct calculation of the electrostatic potential at the heme pocket, by solving the Poisson–Boltzmann equation for a CO ligand of the heme in horse heart and yeast cytochrome c.[193]

As mentioned above, electric fields can control kinetics and thermodynamics of chemical reactions catalyzed by heme proteins. DFT simulations were applied to investigate the effects induced by moderately strong electric fields on the selectivity of two competing nonpolar bond activation processes, C–H hydroxylation and C=C epoxidation, promoted by the active species of cytochrome P450.[194] These authors found that the direction of the field drives the reaction path, which otherwise would not exhibit selectivity between complete hydroxylation and complete epoxidation.

A strategy for mimicking the effects of the electric field at lipid bilayer membranes consists in immobilizing the proteins on self-assembled monolayers (SAM) over electrode surfaces. Structural information may be experimentally obtained by means of resonance Raman and surface-enhanced resonance Raman spectroscopy (SERRS) experiments.[195] A limitation of this approach is that the magnitudes of the local field at the active site are not trivial to assess. In this context, molecular dynamics simulations may provide insight not accessible experimentally. Electric field induced shifts in the redox potentials of tetraheme cytochromes c3 (cyt-c3) inmobilized on SAM were studied by SERRS and molecular dynamics techniques.[195] The MD simulations predicted that the redox potentials of the four hemes of cyt-c3 are affected upon binding to the SAM producing shifts in the redox potentials up to −160 mV, consistent with the experimental results.[195]

6. Conclusions and future prospects

The present results make apparent the contribution of computational classical, quantum mechanical, and hybrid quantum-classical techniques to the exploration of the molecular basis of heme proteins function. In particular, it has been shown how structural and conformational features and ligand migration paths can be investigated with classical MD simulations in combination with advanced sampling tools, such as MSMD, to yield information about free energy barriers and possible secondary docking sites. On the other hand, it was argued that QM-MM tools are specially suited to investigate the protein influence (proximal and distal effects) on the heme active site reactivity. These two frameworks, classical MD and QM-MM, by covering different time and space scales, complement each other in providing a complete picture of the protein function. The agreement with the experimental data, when available, constitutes a stringent test to the reliability of these approaches. Computational simulation is a precious tool even if it is often used to validate and contrast experimental observations, because it offers a microscopic view, sometimes resolved in real time, as no other method is capable to provide. With the refinement of the methodology and the hardware, classical and QM-MM simulation will be more and more at the center of the stage in structural and molecular biology, likely to become an independent tool with the same hierarchy as any experimental technique.

Acknowledgements

This work was partially supported by the University of Buenos Aires, Agencia Nacional de Promoción Científica y Tecnológica (project PICT 06-08447), CONICET (PIP 02508), and Fundación Antorchas.

References

1 S. Kundu, J. T. Trent, 3rd and M. S. Hargrove, *Trends Plant Sci.*, 2003, **8**, 387–393.
2 G. Simonneaux and A. Bondon, *Chem. Rev.*, 2005, **105**, 2627–2646.
3 S. Shaik, D. Kumar, S. P. de Visser, A. Altun and W. Thiel, *Chem. Rev.*, 2005, **105**, 2279–2328.
4 R. Jain and M. K. Chan, *J. Biol. Inorg. Chem.*, 2003, **8**, 1–11.
5 D. A. Pearlman, D. A. Case, J. W. Caldwell, W. S. Ross, T. E. Cheatham Iii, S. DeBolt, D. Ferguson, G. Seibel and P. Kollman, *Comput. Phys. Commun.*, 1995, **91**, 1–41.
6 A. D. MacKerell, Jr, D. Bashford, M. Bellott, R. L. Dunbrack, Jr, J. D. Evanseck, M. J. Field, S. Fischer, J. Gao, H. Guo, S. Ha, D. Joseph-McCarthy, L. Kuchnir, K. Kuczera, F. T. K. Lau, C. Mattos, S. Michnick, T. Ngo, D. T. Nguyen, B. Prodhom, W. E. Reiher Iii, B. Roux, M. Schlenkrich, J. C. Smith, R. Stote, J. Straub, M. Watanabe, J. Wiórkiewicz-Kuczera, D. Yin and M. Karplus, *J. Phys. Chem. B*, 1998, **102**, 3586–3616.
7 W. F. Van Gunsteren and H. J. C. Berendsen, *Angew. Chem., Int. Ed. Engl.*, 1990, **29**, 992–1023.
8 A. Laio and M. Parrinello, *Proc. Natl. Acad. Sci. U. S. A.*, 2002, **99**, 12562–12566.
9 M. Andrec, A. K. Felts, E. Gallicchio and R. M. Levy, *Proc. Natl. Acad. Sci. U. S. A.*, 2005, **102**, 6801–6806.
10 S. Park and K. Schulten, *J. Chem. Phys.*, 2004, **120**, 5946–5961.
11 G. Monard and K. M. Merz, Jr, *Acc. Chem. Res.*, 1999, **32**, 904–911.
12 U. Ryde, *Curr. Opin. Chem. Biol.*, 2003, **7**, 136–142.
13 R. A. Friesner and V. Guallar, *Annu. Rev. Phys. Chem.*, 2005, **56**, 389–427.
14 R. Elber and M. Karplus, *Science*, 1987, **235**, 318–321.
15 C. L. Brooks III, *J. Mol. Biol.*, 1992, **227**, 375–380.
16 J. Tirado-Rives and W. L. Jorgensen, *Biochemistry*, 1993, **32**, 4175–4184.
17 R. Elber and M. Karplus, *J. Am. Chem. Soc.*, 1990, **112**, 9161–9175.
18 K. Kuczera, J. C. Lambry, J. L. Martin and M. Karplus, *Proc. Natl. Acad. Sci. U. S. A.*, 1993, **90**, 5805–5807.
19 J. Ma, S. Huo and J. E. Straub, *J. Am. Chem. Soc.*, 1997, **119**, 2541–2551.
20 K. Kuczera, J. Kuriyan and M. Karplus, *J. Mol. Biol.*, 1990, **213**, 351–373.
21 R. J. Loncharich and B. R. Brooks, *J. Mol. Biol.*, 1990, **215**, 439–455.
22 C. Kiefl, N. Sreerama, R. Haddad, L. Sun, W. Jentzen, Y. Lu, Y. Qiu, J. A. Shelnutt and R. W. Woody, *J. Am. Chem. Soc.*, 2002, **124**, 3385–3394.
23 E. R. Henry, *Biophys. J.*, 1993, **64**, 869–885.
24 A. S. F. Oliveira, V. H. Teixeira, A. M. Baptista and C. M. Soares, *Biophys. J.*, 2005, **89**, 3919–3930.
25 C. M. Soares, P. J. Martel, J. Mendes and M. A. Carrondo, *Biophys. J.*, 1998, **74**, 1708–1721.
26 C. Bret, M. Roth, S. Nørager, E. C. Hatchikian and M. J. Field, *Biophys. J.*, 2002, **83**, 3049–3065.
27 E. R. Henry, M. Levitt and W. A. Eaton, *Proc. Natl. Acad. Sci. U. S. A.*, 1985, **82**, 2034–2038.
28 D. Vitkup, G. A. Petsko and M. Karplus, *Nat. Struct. Biol.*, 1997, **4**, 202–208.
29 J. Kottalam and D. A. Case, *J. Am. Chem. Soc.*, 1988, **110**, 7690–7697.
30 R. Czerminski and R. Elber, *Proteins: Struct., Funct., Genet.*, 1991, **10**, 70–80.
31 M. L. Carlson, R. M. Regan and Q. H. Gibson, *Biochemistry*, 1996, **35**, 1125–1136.
32 S. K. Ludemann, V. Lounnas and R. C. Wade, *J. Mol. Biol.*, 2000, **303**, 797–811.
33 C. Bossa, M. Anselmi, D. Roccatano, A. Amadei, B. Vallone, M. Brunori and A. Di Nola, *Biophys. J.*, 2004, **86**, 3855–3862.
34 C. Bossa, A. Amadei, I. Daidone, M. Anselmi, B. Vallone, M. Brunori and A. D. Nola, *Biophys. J.*, 2005, **89**, 465–474.
35 S. Y. Sheu, *J. Chem. Phys.*, 2005, **122**, 1–7.
36 M. Brunori, F. Cutruzzola, C. Savino, C. Travaglini-Allocatelli, B. Vallone and Q. H. Gibson, *Biophys. J.*, 1999, **76**, 1259–1269.
37 G. Hummer, F. Schotte and P. A. Anfinrud, *Proc. Natl. Acad. Sci. U. S. A.*, 2004, **101**, 15330–15334.
38 S. G. Kalko, J. L. Gelpi, I. Fita and M. Orozco, *J. Am. Chem. Soc.*, 2001, **123**, 9665–9672.
39 S. K. Ludemann, V. Lounnas and R. C. Wade, *J. Mol. Biol.*, 2000, **303**, 813–830.
40 P. Banushkina and M. Meuwly, *J. Phys. Chem. B*, 2005, **109**, 16911–16917.
41 C. Jarzynski, *Phys. Rev. Lett.*, 1997, **78**, 2690–2693.
42 W. Li, H. Liu, E. E. Scott, F. Grater, J. R. Halpert, X. Luo, J. Shen and H. Jiang, *Drug Metab. Dispos.*, 2005, **33**, 910–919.
43 A. Bidon-Chanal, M. A. Marti, A. Crespo, M. Milani, M. Orozco, M. Bolognesi, F. J. Luque and D. A. Estrin, *Proteins: Struct., Funct., Bioinform.*, 2006.
44 H. Ouellet, Y. Ouellet, C. Richard, M. Labarre, B. Wittenberg, J. Wittenberg and M. Guertin, *Proc. Natl. Acad. Sci. U. S. A.*, 2002, **99**, 5902–5907.
45 M. Milani, A. Pesce, Y. Ouellet, P. Ascenzi, M. Guertin and M. Bolognesi, *EMBO J.*, 2001, **20**, 3902–3909.
46 L. Mouawad, J. D. Maréchal and D. Perahia, *Bioch. Biophys. Acta*, 2005, **1724**, 385–393.
47 N. Ramadas and J. M. Rifkind, *Biophys. J.*, 1999, **76**, 1796–1811.
48 (*a*) L. Mouawad, D. Perahia, C. H. Robert and C. Guilbert, *Biophys. J.*, 2002, **82**, 3224–3245; (*b*) L. Mouawad and D. Perahia, *J. Mol. Biol.*, 1996, **258**, 393–410; (*c*) L. Mouawad and D. Perahia, *Biopolymers*, 1993, **33**, 599–611; (*d*) D. Perahia and L. Mouawad, *Comput. Chem.*, 1995, **19**, 241–246.
49 M. Falconi, A. Desideri, A. Cupane, M. Leone, G. Ciccotti, E. S. Peterson, J. M. Friedman, A. Gambacurta and F. Ascoli, *Biophys. J.*, 1998, **75**, 2489–2503.
50 Y. Zhou, H. Zhou and M. Karplus, *J. Mol. Biol.*, 2003, **326**, 593–606.
51 T. Persichini, V. Mazzone, F. Polticelli, S. Moreno, G. Venturini, E. Clementi and M. Colasanti, *Neurosci. Lett.*, 2005, **384**, 254–259.
52 V. Lounnas, B. M. Pettitt and G. N. Phillips, Jr, *Biophys. J.*, 1994, **66**, 601–614.
53 G. N. Phillips, Jr and B. M. Pettitt, *Protein Sci.*, 1995, **4**, 149–158.
54 W. Gu and B. P. Schoenborn, *Proteins: Struct., Funct., Genet.*, 1995, **22**, 20–26.
55 D. E. Stewart and J. E. Wampler, *Proteins*, 1991, **11**, 142–152.
56 P. J. Steinbach and B. R. Brooks, *Proc. Natl. Acad. Sci. U. S. A.*, 1993, **90**, 9135–9139.
57 J. C. Smith, F. Merzel, A. N. Bondar, A. Tournier and S. Fischer, *Philos. Trans. R. Soc. London, Ser. B*, 2004, **359**, 1181–1189; discussion 1189–1190.
58 W. Gu, A. E. Garcia and B. P. Schoenborn, *Basic Life Sci.*, 1996, **64**, 289–298.
59 V. A. Makarov, M. Feig, B. K. Andrews and B. M. Pettitt, *Biophys. J.*, 1998, **75**, 150–158.
60 V. A. Makarov, B. K. Andrews, P. E. Smith and B. M. Pettitt, *Biophys. J.*, 2000, **79**, 2966–2974.
61 G. Cottone, L. Cordone and G. Ciccotti, *Biophys. J.*, 2001, **80**, 931–938.
62 G. Cottone, S. Giuffrida, G. Ciccotti and L. Cordone, *Proteins: Struct., Funct., Gen.*, 2005, **59**, 291–302.
63 L. Cordone, G. Cottone, S. Giuffrida, G. Palazzo, G. Venturoli and C. Viappiani, *Biochim. Biophys. Acta*, 2005, **1749**, 252–281.
64 O. Schaad, H. X. Zhou, A. Szabo, W. A. Eaton and E. R. Henry, *Proc. Natl. Acad. Sci. U. S. A.*, 1993, **90**, 9547–9551.
65 M. Meuwly, O. M. Becker, R. Stote and M. Karplus, *Biophys. Chem.*, 2002, **98**, 183–207.
66 D. R. Nutt and M. Meuwly, *Biophys. J.*, 2006, **90**, 1191–1201.
67 G. H. Loew and D. L. Harris, *Chem. Rev.*, 2000, **100**, 407–419.
68 J. P. Collman, J. L. Hoard, N. Kim, G. Lang and C. A. Reed, *J. Am. Chem. Soc.*, 1975, **97**, 2676–2681.
69 G. Lang, K. Spartalian, C. A. Reed and J. P. Collman, *J. Chem. Phys.*, 1978, **69**, 5424–5427.
70 P. D. W. Boyd, A. D. Buckingham, R. M. McMecking and S. Mitra, *Inorg. Chem.*, 1979, **18**, 3585–3591.
71 H. Goff, G. N. La Mar and C. A. Reed, *J. Am. Chem. Soc.*, 1977, **99**, 3641–3646.
72 J. Mispelter, M. Momenteau and J. M. Lhoste, *J. Chem. Phys.*, 1980, **72**, 1003–1012.
73 W. R. Scheidt and C. A. Reed, *Chem. Rev.*, 1981, **81**, 543–555.

74 C. Rovira, K. Kunc, J. Hutter, P. Ballone and M. Parrinello, *J. Phys. Chem. A*, 1997, **101**, 8914–8925.
75 D. A. Scherlis and D. A. Estrin, *Int. J. Quantum Chem.*, 2002, **87**, 158.
76 S. Franzen, *Proc. Natl. Acad. Sci. U. S. A.*, 2002, **99**, 16754–16759.
77 A. Ghosh and P. R. Taylor, *Curr. Opin. Chem. Biol.*, 2003 **7**, 113.
78 P. M. Kozlowski, T. G. Spiro and M. Z. Zgierski, *J. Phys. Chem. B*, 2000, **104**, 10659–10666.
79 M. S. Liao and S. Scheiner, *J. Chem. Phys.*, 2002, **116**, 3635–3645.
80 J. N. Harvey, *Struct. Bonding*, 2004, **112**, 151–183.
81 (*a*) R. J. Deeth and N. Fey, *J. Comput. Chem.*, 2004, **25**, 1840–1848; (*b*) D. M. A. Smith, M. Dupuis and T. P. Straatsma, *Mol. Phys.*, 2005, **103**, 273.
82 M. Cococcioni and S. De Gironcoli, *Phys. Rev. B*, 2005, **71**, 1–16.
83 H. Kullik, M. Cococcioni, D. A. Scherlis and N. Marzari, *Phys. Rev. Lett.*, 2006, **97**, 103001–103004.
84 D. A. Scherlis, M. Cococcioni, P. Sit and N. Marzari, to be submitted.
85 (*a*) T. Uchida and T. Kitagawa, *Acc. Chem. Res.*, 2005, **38**, 662–670; (*b*) L. M. Miller, A. J. Pedraza and M. R. Chance, *Biochemistry*, 1997, **36**, 12199–12207.
86 J. M. Soler, E. Artacho, J. D. Gale, A. García, J. Junquera, P. Ordejón and D. Sánchez-Portal, *J. Phys.: Condens. Matter*, 2002, **14**, 2745–2779.
87 J. P. Perdew, K. Burke and M. Ernzerhof, *Phys. Rev. Lett.*, 1996, **77**, 3865–3868.
88 A. Crespo, D. A. Scherlis, M. A. Marti, P. Ordejón, A. E. Roitberg and D. A. Estrin, *J. Phys. Chem. B*, 2003, **107**, 13728–13736.
89 J. Wang, P. Cieplak and P. A. Kollman, *J. Comput. Chem.*, 2000, **21**, 1049–1074.
90 L. Capece, M. Marti, A. Crespo, F. Doctorovich and D. Estrin, *J. Am. Chem. Soc.*, 2006, **128**, 12455–12461.
91 G. B. Jameson, G. A. Rodley, W. T. Robinson, R. R. Gagne, C. A. Reed and J. A. Collman, *Inorg. Chem.*, 1978, **17**, 850–857.
92 A. Crespo, M. A. Marti, S. G. Kalko, A. Morreale, M. Orozco, J. L. Gelpi, F. J. Luque and D. A. Estrin, *J. Am. Chem. Soc.*, 2005, **127**, 4433–4444.
93 (*a*) C. Rovira and M. Parrinello, *Biophys. J.*, 2000, **78**, 93–100; (*b*) C. Rovira, B. Schulze, M. Eichinger, J. D. Evanseck and M. Parrinello, *Biophys. J.*, 2001, **81**, 435–445.
94 J. P. Collman, J. I. Brauman, T. R. Halbert and K. S. Suslick, *Proc. Natl. Acad. Sci. U. S. A.*, 1976, **73**, 3333–3337.
95 A. Ghosh and D. F. Bocian, *J. Chem. Phys.*, 1996, **100**, 6363–6367.
96 T. G. Spiro and P. M. Kozlowski, *Acc. Chem. Res.*, 2001, **34**, 137–144.
97 T. Vangberg, D. F. Bocian and A. Ghosh, *J. Biol. Inorg. Chem.*, 1997, **2**, 526–530.
98 T. G. Spiro and I. H. Wasbotten, *J. Inorg. Biochem.*, 2005, **99**, 34–44.
99 G. N. Phillips, Jr, M. L. Teodoro, T. Li, B. Smith and J. S. Olson, *J. Phys. Chem. B*, 1999, **103**, 8817–8829.
100 T. Uno, Y. Nishimura, M. Tsuboi, R. Makino, T. Iizuka and Y. Ishimura, *J. Biol. Chem.*, 1987, **262**, 4549–4556.
101 M. Tsubaki and Y. Ichikawa, *Biochim. Biophys. Acta*, 1985, **827**, 268–274.
102 K. M. Vogel, P. M. Kozlowski, M. Z. Zgierski and T. G. Spiro, *Inorg. Chim. Acta*, 2000, **297**, 11–17.
103 M. K. Ellison, C. E. Schulz and W. R. Scheidt, *J. Am. Chem. Soc.*, 2002, **124**, 13833–13841.
104 J. H. Enemark and R. D. Feltham, *Coord. Chem. Rev.*, 1974, **13**, 339–406.
105 D. P. Linder and K. R. Rodgers, *Inorg. Chem.*, 2005, **44**, 1367–1380.
106 W. R. Scheidt and P. L. Piciulo, *J. Am. Chem. Soc.*, 1976, **98**, 1913–1919.
107 L. E. Laverman and P. C. Ford, *J. Am. Chem. Soc.*, 2001, **123**, 11614–11622.
108 J. W. Denninger and M. A. Marletta, *Biochem. Biophys. Acta*, 1999, **1411**, 334–350.
109 J. P. M. Schelvis, S. A. Seibold, J. F. Cerda, R. M. Garavito and G. T. Babcock, *J. Phys. Chem. B*, 2000, **104**, 10844–10850.
110 C. R. Andrew, E. L. Green, D. M. Lawson and R. R. Eady, *Biochemistry*, 2001, **40**, 4115–4122.
111 D. S. Karow, D. Pan, R. Tran, P. Pellicena, A. Presley, R. A. Mathies and M. A. Marletta, *Biochemistry*, 2004, **43**, 10203–10211.
112 D. P. Ballou, Y. Zhao, P. E. Brandish and M. A. Marletta, *Proc. Natl. Acad. Sci. U. S. A.*, 2002, **99**, 12097–12101.
113 Y. Zhao, P. E. Brandish, D. P. Ballou and M. A. Marletta, *Proc. Natl. Acad. Sci. U. S. A.*, 1999, **96**, 14753–14758.
114 T. C. Bellamy, J. Wood and J. Garthwaite, *Proc. Natl. Acad. Sci. U. S. A.*, 2002, **99**, 507–510.
115 M. A. Marti, L. Capece, A. Crespo, F. Doctorovich and D. A. Estrin, *J. Am. Chem. Soc.*, 2005, **127**, 7721–7728.
116 V. S. Sharma, T. G. Traylor, R. Gardiner and H. Mizukami, *Biochemistry*, 1987, **26**, 3837–3843.
117 F. A. Walker, *J. Inorg. Biochem.*, 2005, **99**, 216–236.
118 D. E. Champagne, R. H. Nussenzveig and J. M. C. Ribeiro, *J. Biol. Chem.*, 1995, **270**, 8691–8695.
119 A. Weichsel, J. F. Andersen, S. A. Roberts and W. R. Montfort, *Nat. Struct. Biol.*, 2000, **7**, 551–554.
120 T. Wondimagegn and A. Ghosh, *J. Am. Chem. Soc.*, 2001, **123**, 1543–1544.
121 A. J. Hobbs, J. M. Fukuto and L. J. Ignarro, *Proc. Natl. Acad. Sci. U. S. A.*, 1994, **91**, 10992–10996.
122 S. Adak, Q. Wang and D. J. Stuehr, *J. Biol. Chem.*, 2000, **275**, 17434–17439.
123 H. H. Schmidt, H. Hofmann, U. Schindler, Z. S. Shutenko, D. D. Cunningham and M. Feelisch, *Proc. Natl. Acad. Sci. U. S. A.*, 1996, **93**, 14492–14497.
124 P. Pagliaro, *Life Sci.*, 2003, **73**, 2137–2149.
125 D. A. Wink, K. M. Miranda, T. Katori, D. Mancardi, D. D. Thomas, L. Ridnour, M. G. Espey, M. Feelisch, C. A. Colton, J. M. Fukuto, P. Pagliaro, D. A. Kass and N. Paolocci, *Am. J. Physiol.: Heart Circ. Physiol.*, 2003, **285**, H2264–2276.
126 P. Pagliaro, D. Mancardi, R. Rastaldo, C. Penna, D. Gattullo, K. M. Miranda, M. Feelisch, D. A. Wink, D. A. Kass and N. Paolocci, *Free Radical Biol. Med.*, 2003, **34**, 33–43.
127 N. Paolocci, T. Katori, H. C. Champion, M. E. St John, K. M. Miranda, J. M. Fukuto, D. A. Wink and D. A. Kass, *Proc. Natl. Acad. Sci. U. S. A.*, 2003, **100**, 5537–5542.
128 K. M. Miranda, N. Paolocci, T. Katori, D. D. Thomas, E. Ford, M. D. Bartberger, M. G. Espey, D. A. Kass, M. Feelisch, J. M. Fukuto and D. A. Wink, *Proc. Natl. Acad. Sci. U. S. A.*, 2003, **100**, 9196–9201.
129 D. A. Bazylinski and T. C. Hollocher, *J. Am. Chem. Soc.*, 1985, **107**, 7982–7986.
130 D. A. Bazylinski, J. Goretski and T. C. Hollocher, *J. Am. Chem. Soc.*, 1985, **107**, 7986–7989.
131 M. P. Doyle, S. N. Mahapatro, R. D. Broene and J. K. Guy, *J. Am. Chem. Soc.*, 1988, **110**, 593–599.
132 K. M. Miranda, R. W. Nims, D. D. Thomas, M. G. Espey, D. Citrin, M. D. Bartberger, N. Paolocci, J. M. Fukuto, M. Feelisch and D. A. Wink, *J. Inorg. Biochem.*, 2003, **93**, 52–60.
133 C. E. Immoos, F. Sulc, P. J. Farmer, K. Czarnecki, D. F. Bocian, A. Levina, J. B. Aitken, R. S. Armstrong and P. A. Lay, *J. Am. Chem. Soc.*, 2005, **127**, 814–815.
134 P. R. Gardner, A. M. Gardner, W. T. Brashear, T. Suzuki, A. N. Hvitved, K. D. Setchell and J. S. Olson, *J. Inorg. Biochem.*, 2006, **100**, 542–550.
135 L. M. Blomberg, M. R. Blomberg and P. E. Siegbahn, *J. Biol. Inorg. Chem.*, 2004, **9**, 923–935.
136 D. Ostovic and T. C. Bruice, *Acc. Chem. Res.*, 1992, **25**, 314–320.
137 B. Meunier, *Chem. Rev.*, 1992, **92**, 1411–1456.
138 J. T. Groves and Y. Z. Hang, in *Cytochrome P450: Structure, Mechanism and Biochemistry*, ed. P. R. Ortiz de Montellano, Plenum Press, New York, 2nd edn, 1995.
139 M. Sono, M. P. Roach, E. D. Coulter and J. H. Dawson, *Chem. Rev.*, 1996, **96**, 2841–2888.
140 P. R. Ortiz De Montellano, *Acc. Chem. Res.*, 1998, **31**, 543–549.
141 M. Newcomb and P. H. Toy, *Acc. Chem. Res.*, 2000, **33**, 449–455.
142 J. T. Groves, *J. Chem. Educ.*, 1985, **62**, 928–931.
143 J. H. Dawson, *Science*, 1988, **240**, 433–439.
144 D. Goldfarb, M. Bernardo, H. Thomann, P. M. H. Kroneck and V. Ullrich, *J. Am. Chem. Soc.*, 1996, **118**, 2686–2693.
145 P. H. Toy, B. Dhanabalasingam, M. Newcomb, I. H. Hanna and P. F. Hollenberg, *J. Org. Chem.*, 1997, **62**, 9114–9122.

146 D. L. Wertz, M. F. Sisemore, M. Selke, J. Driscoll and J. S. Valentine, *J. Am. Chem. Soc.*, 1998, **120**, 5331–5332.
147 P. H. Toy, M. Newcomb and P. F. Hollenberg, *J. Am. Chem. Soc.*, 1998, **120**, 7719–7729.
148 J. Hart-Davis, P. Battioni, J. L. Boucher and D. Mansuy, *J. Am. Chem. Soc.*, 1998, **120**, 12524–12530.
149 Z. Gross, S. Nimri, C. M. Barzilay and L. Simkhovich, *J. Biol. Inorg. Chem.*, 1997, **2**, 492–506.
150 R. Davydov, T. M. Makris, V. Kofman, D. E. Werst, S. G. Sligar and B. M. Hoffman, *J. Am. Chem. Soc.*, 2001, **123**, 1403–1415.
151 J. T. Groves and G. A. McClusky, *J. Am. Chem. Soc.*, 1976, **98**, 859–861.
152 J. T. Groves and M. Van Der Puy, *J. Am. Chem. Soc.*, 1976, **98**, 5290–5297.
153 J. T. Groves and D. V. Subramanian, *J. Am. Chem. Soc.*, 1984, **106**, 2177–2181.
154 D. L. Harris and G. H. Loew, *J. Am. Chem. Soc.*, 1998, **120**, 8941–8948.
155 M. T. Green, *J. Am. Chem. Soc.*, 1999, **121**, 7939–7940.
156 J. C. Schöneboom, H. Lin, N. Reuter, W. Thiel, S. Cohen, F. Ogliaro and S. Shaik, *J. Am. Chem. Soc.*, 2002, **124**, 8142–8151.
157 S. Shaik, M. Filatov, D. Schröder and H. Schwarz, *Chem.–Eur. J.*, 1998, **4**, 193–199.
158 I. Schlichting, J. Berendzen, K. Chu, A. M. Stock, S. A. Maves, D. E. Benson, R. M. Sweet, D. Ringe, G. A. Petsko and S. G. Sligar, *Science*, 2000, **287**, 1615–1622.
159 J. T. Groves, Z. Gross and M. K. Stern, *Inorg. Chem.*, 1994, **33**, 5065–5072.
160 J. T. Groves and Y. Watanabe, *J. Am. Chem. Soc.*, 1988, **110**, 8443–8452.
161 J. P. Collman, J. I. Brauman, P. D. Hampton, H. Tanaka, D. S. Bohle and R. T. Hembre, *J. Am. Chem. Soc.*, 1990, **112**, 7980–7984.
162 D. Schröder, S. Shaik and H. Schwarz, *Acc. Chem. Res.*, 2000, **33**, 139–145.
163 F. Ogliaro, S. P. de Visser, J. T. Groves and S. Shaik, *Angew. Chem., Int. Ed.*, 2001, **40**, 2874–2878.
164 S. Shaik, S. P. De Visser, F. Ogliaro, H. Schwarz and D. Schröder, *Curr. Opin. Chem. Biol.*, 2002, **6**, 556–567.
165 P. K. Sharma, S. P. De Visser and S. Shaik, *J. Am. Chem. Soc.*, 2003, **125**, 8698–8699.
166 N. Harris, S. Cohen, M. Filatov, F. Ogliaro and S. Shaik, *Angew. Chem., Int. Ed.*, 2000, **39**, 2003–2007.
167 S. P. De Visser, F. Ogliaro, P. K. Sharma and S. Shaik, *Angew. Chem., Int. Ed.*, 2002, **41**, 1947–1951.
168 F. Ogliaro, N. Harris, S. Cohen, M. Filatov, S. P. De Visser and S. Shaik, *J. Am. Chem. Soc.*, 2000, **122**, 8977–8989.
169 S. P. De Visser, F. Ogliaro, N. Harris and S. Shaik, *J. Am. Chem. Soc.*, 2001, **123**, 3037–3047.
170 F. Ogliaro, S. P. De Visser, S. Cohen, P. K. Sharma and S. Shaik, *J. Am. Chem. Soc.*, 2002, **124**, 2806–2817.
171 J. C. Schöneboom, S. Cohen, H. Lin, S. Shaik and W. Thiel, *J. Am. Chem. Soc.*, 2004, **126**, 4017–4034.
172 V. Guallar, B. F. Gherman, W. H. Miller, S. J. Lippard and R. A. Friesner, *J. Am. Chem. Soc.*, 2002, **124**, 3377–3384.
173 V. Guallar, M. H. Baik, S. J. Lippard and R. A. Friesner, *Proc. Natl. Acad. Sci. U. S. A.*, 2003, **100**, 6998–7002.
174 V. Guallar, V. S. Batista, W. H. Miller and D. L. Harris, *J. Am. Chem. Soc.*, 2002, **124**, 1430–1437.
175 V. Guallar and R. A. Friesner, *J. Am. Chem. Soc.*, 2004, **126**, 8501–8508.
176 T. Kamachi and K. Yoshizawa, *J. Am. Chem. Soc.*, 2003, **125**, 4652–4661.
177 A. Altun, V. Guallar, R. A. Friesner, S. Shaik and W. Thiel, *J. Am. Chem. Soc.*, 2006, **128**, 3924–3925.
178 T. Matsubara, *J. Biochem. (Tokyo)*, 1970, **67**, 229–235.
179 P. R. Alefounder and S. J. Ferguson, *Biochem. J.*, 1980, **192**, 231–240.
180 L. I. Hochstein and G. A. Tomlinson, *Annu. Rev. Microbiol.*, 1988, **42**, 231–261.
181 V. P. Reutov, *Biochemistry (Moscow)*, 2002, **67**, 293–311.
182 Z. Huang, S. Shiva, D. B. Kim-Shapiro, R. P. Patel, L. A. Ringwood, C. E. Irby, K. T. Huang, C. Ho, N. Hogg, A. N. Schechter and M. T. Gladwin, *J. Clin. Invest.*, 2005, **115**, 2099–2107.
183 B. A. Averill and J. M. Tiedje, *FEBS Lett.*, 1982, **138**, 8–12.
184 F. Cutruzzola, K. Brown, E. K. Wilson, A. Bellelli, M. Arese, M. Tegoni, C. Cambillau and M. Brunori, *Proc. Natl. Acad. Sci. U. S. A.*, 2001, **98**, 2232–2237.
185 G. Ranghino, E. Scorza, T. Sjogren, P. A. Williams, M. Ricci and J. Hajdu, *Biochemistry*, 2000, **39**, 10958–10966.
186 M. A. Marti, A. Crespo, S. E. Bari, F. A. Doctorovich and D. A. Estrin, *J. Phys. Chem. B*, 2004, **108**, 18073–18080.
187 T. Kamachi, A. F. Shestakov and K. Yoshizawa, *J. Am. Chem. Soc.*, 2004, **126**, 3672–3673.
188 P. K. Sharma, R. Kevorkiants, S. P. De Visser, D. Kumar and S. Shaik, *Angew. Chem., Int. Ed.*, 2004, **43**, 1129–1132.
189 R. Davydov, T. Matsui, H. Fujii, M. Ikeda-Saito and B. M. Hoffman, *J. Am. Chem. Soc.*, 2003, **125**, 16208–16209.
190 E. S. Park, M. R. Thomas and S. G. Boxer, *J. Am. Chem. Soc.*, 2000, **122**, 12297–12303.
191 S. D. Dalosto, J. M. Vanderkooi and K. A. Sharp, *J. Phys. Chem. B*, 2004, **108**, 6450–6457.
192 A. C. De Dios and E. M. Earle, *J. Phys. Chem. A*, 1997, **101**, 8132–8134.
193 M. Laberge, J. M. Vankerkooi and K. A. Sharp, *J. Phys. Chem.*, 1996, **100**, 10793–10801.
194 S. Shaik, S. P. De Visser and D. Kumar, *J. Am. Chem. Soc.*, 2004, **126**, 11746–11749.
195 L. Rivas, C. M. Soares, A. M. Baptista, J. Simaan, R. E. Di Paolo, D. H. Murgida and P. Hildebrandt, *Biophys. J.*, 2005, **88**, 4188–4199.

